Investigating Phenotypic Changes in Response to Drug Treatments in Epithelial Ovarian Cancer Using a Novel Si-TiB_2 Micropatterned Substrate

by
Margaret Ruth Eisenbrandt

A Thesis submitted to the Biomedical Engineering Department,
Cullen College of Engineering
in partial fulfillment of the requirements for the degree of

Master of Sciences
in Biomedical Engineering

Co-Chair of Committee: Dr. Fatima Merchant

Co-Chair of Committee: Dr. Sheereen Majd

Committee Member: Dr. Wanda Zagozdzon-Wosik

Committee Member: Dr. Muayyad Al-Ubaidi

University of Houston
May 2022

DEDICATION

To Franklin, always my fierce sidekick, for constantly reminding me not to take anything too seriously

ACKNOWLEDGMENTS

I would like to take this opportunity to express my gratitude to my advisor, Dr. Fatima Merchant for giving me this opportunity to grow as a researcher and providing me with dedicated mentorship throughout my graduate studies. I would also like to thank the other members of my thesis committee, Dr. Muayyad Al-Ubaidi, Dr. Sheereen Majd and especially Dr. Wanda Wosik for fabricating the substrates that made this study possible. Additionally, I would like to acknowledge my fellow lab member, Jefferson Friguglietti for lending his expertise and a helping hand whenever I needed it. I also want to thank Maram Quttina for providing her expertise with qPCR assays to help make my project more robust. I would like to thank Dr. Marc Hanke for encouraging me to pursue my passion for biology and research. Of course, I would not be where I am today without the mentors I was lucky to have throughout my primary education who may not realize what a significant impact they had on my confidence as a student and an individual. There are too many to name them all, however I would like to specifically thank Mme Jacqueline Parr, Mrs. Cathy Gunvalson, Mrs. Pamela Bloom, Mme Amy Budion, Mr. Doug Long, Mrs. Cathy Meyer and Mrs. Nicole Malone. You have all made a difference by being dedicated, passionate educators and I hope you know your efforts are greatly appreciated. Finally, I would like to thank my family and friends for being there for me through this entire journey, I would not have been able to do any of this without your support.

ABSTRACT

Epithelial ovarian cancer (EOC) is one of the most prevalent cancers in women worldwide, with nearly 80% of cases diagnosed in late-stage of disease and an overall survival rate of less than 50%. 3D culture is necessary in order to study the *in vivo* response of cancer cells to therapeutic agents, in systems that better mimic innate cell-cell and cell-ECM interactions. This study evaluates the potential of a novel micropatterned substrate, fabricated using photolithography to deposit TiB_2 micropatterns onto a Si wafer to study the response of EOC to epigenetic and chemotherapeutic drugs. Previous work has validated that the Si-TiB_2 substrate enables selective deposition of growth factors and self-assembly of cells onto the TiB_2 pattern through differences in stiffness, roughness, wetness, and charge gradient. For EOC cell lines, OVCAR3 (low invasiveness) and SKOV3 (high invasiveness), the Si-TiB_2 micropatterned substrate supported cell proliferation and maintained viability, and 3D aggregation for SKOV3 cells. Treating SKOV3 aggregates and OVCAR3 monolayers on patterned substrates, with an epigenetic drug, vorinostat, also known as suberoylanilide hydroxamic acid (SAHA), resulted in decreased diameter and thickness, however viability of the remaining cells was unchanged. Genomic analysis of the treated aggregates suggests a change in phenotype of SKOV3 after treatment with SAHA. While studies show that SAHA alone may not be a sufficient treatment for EOC, it does have the potential to augment the treatment of some cancers when used in combination with chemotherapeutic agents. Treatment of SKOV3 aggregates with a combination of SAHA and Paclitaxel was shown to decrease proliferation and halt growth for an extended period after treatment however these results are not statistically different from

the Paclitaxel treatment group, which agrees with a clinical trial of SAHA and Paclitaxel combinatorial treatment. Collectively, data support use of the micropatterned substrate for investigation of potential drug therapies for cancer treatment and cellular changes in response to drug treatment.

TABLE OF CONTENTS

LIST OF TABLES

LIST OF FIGURES

Chapter 1 Introduction and Background

In 2020 the reported number of new ovarian cancer diagnoses worldwide was 313,595 resulting in 207,252 deaths making ovarian cancer the eighth-most diagnosed cancer in women. Additionally, ovarian cancer is the fifth leading cause of cancer related death for women and of all diagnosed cases over 90% are epithelial ovarian cancer (EOC) [1]–[4]. EOC can be further differentiated into histological subtypes including serous, endometrioid, mucinous and clear cell carcinoma, as seen in Figure 1.

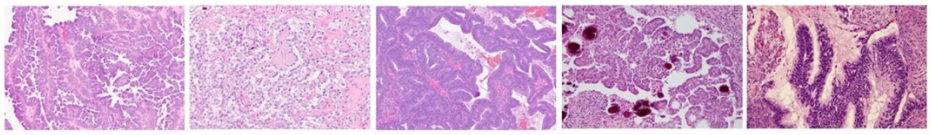

	High-Grade Serous Carcinoma	Clear Cell Carcinoma	Endometrioid Carcinoma	Low-Grade Serous Carcinoma	Mucinous Carcinoma
% of all Ovarian Carcinomas	~70%	~10%	~10%	<5%	<5%
Precursor Lesions	Serous tubal intraepithelial carcinoma (STIC)	Clear Cell Borderline Tumor	Endometrioid Borderline Tumor	Serous Borderline Tumor	Mucinous Borderline Tumor

Figure 1. Histological classifications of epithelial ovarian cancer [5].

The Federation of Gynecology and Obstetrics (FIGO) has developed a ranking for endometrial and cervical cancers, which places cancers on a scale from 0-IV with stages III-IV considered late-stage [2]. Cases of serous carcinoma make up more than half of EOC diagnoses and 80% of these are diagnosed at stage III or IV, while the other EOC subtypes are primarily diagnosed at stage I [1]. The high rates of late-stage diagnosis are linked to the lack of early detection tools as well as the aggressiveness of certain EOC subtypes. Late-stage diagnosis is correlated to high rates of relapse, heavy tumor burdens and drug resistance, making EOC treatment incredibly challenging and resulting in poor prognosis for many patients (Figure 2).

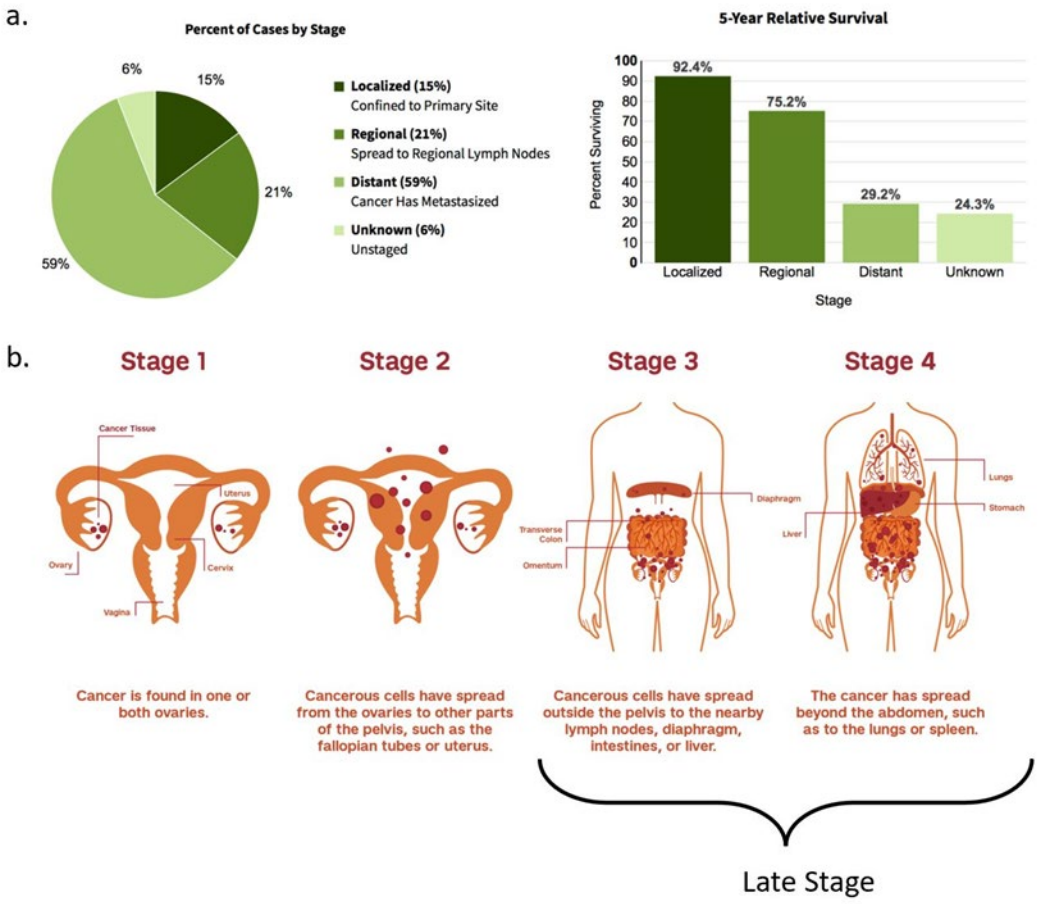

Figure 2. (A) Ovarian cancer diagnosis and 5 year survival statistics [6]. (B) Stages of ovarian cancer [7].

The most common initial treatment for EOC is surgery to remove as much of the tumor(s) as possible, followed by chemotherapeutic agents, often cisplatin or Paclitaxel, to ensure that any remaining cancer cells are eliminated [8]. Although this treatment plan can provide extended life expectancy, the 5-year survival rate for all ovarian cancer patients is less than 50% [4]. This lack of effectiveness can be attributed to the heterogeneity and resultant chemoresistance in some subpopulations of EOC cells [8]. In some cases when patients present with very large tumors chemotherapy may precede surgery to first shrink the tumor before removal, however, generally

chemotherapy is primarily useful in killing remaining cancer cells rather than clumped aggregates.

While chemotherapeutic agents are often effective at killing remaining cells, in EOC patients there are high rates of relapse, particularly because late-stage diagnosis occurs in 70% of cases [1]. Treatment of EOC with only one drug can potentially contribute to drug resistance and in cases of relapse and late diagnoses drug resistance is a prevalent concern, hence there is currently a discussion surrounding the potential benefits of combinatorial treatments to improve treatment outcomes in EOC patients [9], [10]. There have been several studies into the efficacy of Histone Deacetylase inhibitors (HDIs) as a method of sensitizing EOC cells to chemotherapeutics to which they have demonstrated some level of resistance. HDIs are epigenetic drug therapies that have been shown to work by suppressing transcription through histone deacetylation, resulting in chromatin decompaction which leads to alterations in gene transcription [11]–[14] (Figure 3). Suberoylanilide hydroxamic acid (SAHA) is one HDI that has been shown to increase cell sensitivity to drugs like cisplatin and other chemotherapeutics in EOC solid tumors [9], [11]–[16]. SAHA is currently only approved to augment treatment of cutaneous manifestations in T-cell lymphoma patients that have recurring disease, however the demonstrated efficacy in these cases provides some hope that SAHA could be used as an augmentative to EOC treatments.

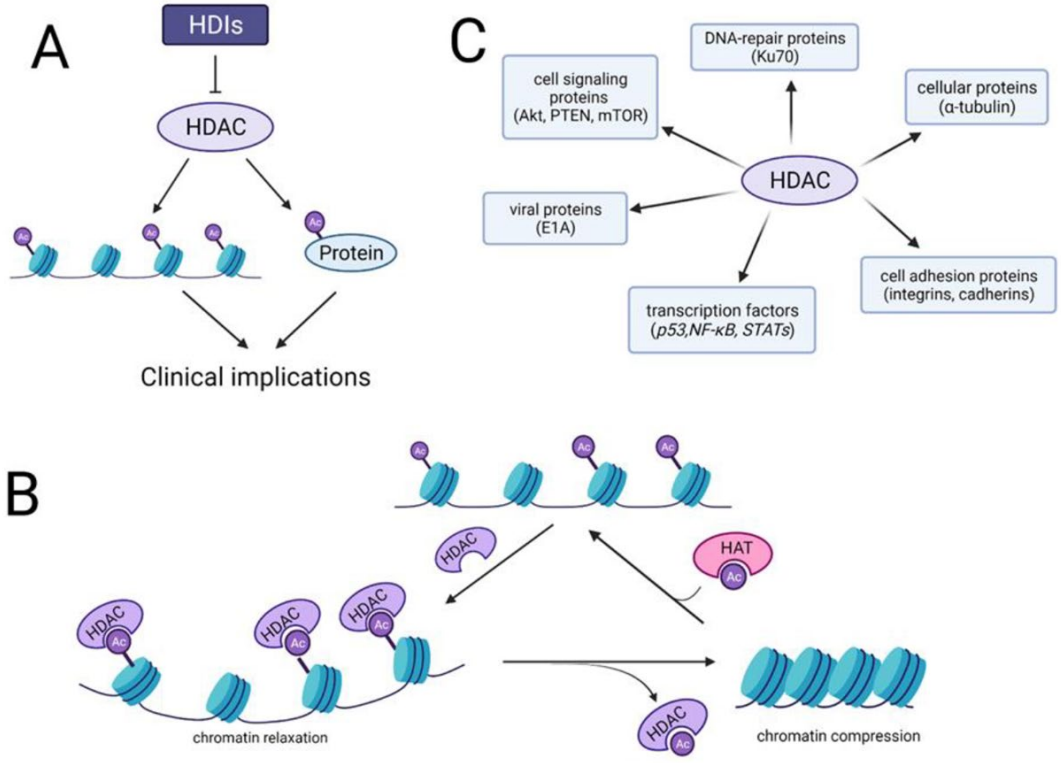

Figure 3. (A) Histone Deacetylase Inhibitors role in DNA transcription. (B) Schematic of the normal function of Histone Deacetylase. (C) The many biological pathways that Histone Deacetylase are involved in [13].

Paclitaxel is a common chemotherapeutic used in EOC treatment and its mode of action involves induction of cell cycle arrest in either M phase or G0 and G1/S at high and low concentrations respectively. Additionally, studies into the Paclitaxel resistance of patient derived EOC cells has shown that cell populations that are resistant to Paclitaxel are not resistant to SAHA, demonstrating a promising combination treatment [9] (Figure 4). There have been several studies assessing the effects of SAHA and Paclitaxel combinations in EOC patients. Studies in mice using SKOV3 and patient derived EOC cells injected intraperitoneally demonstrate similar results, showing a relatively equal response to SAHA and Paclitaxel, however there is some disagreement

as to whether or not the combination results in an additive effect that is statistically significant [9], [15]–[18].

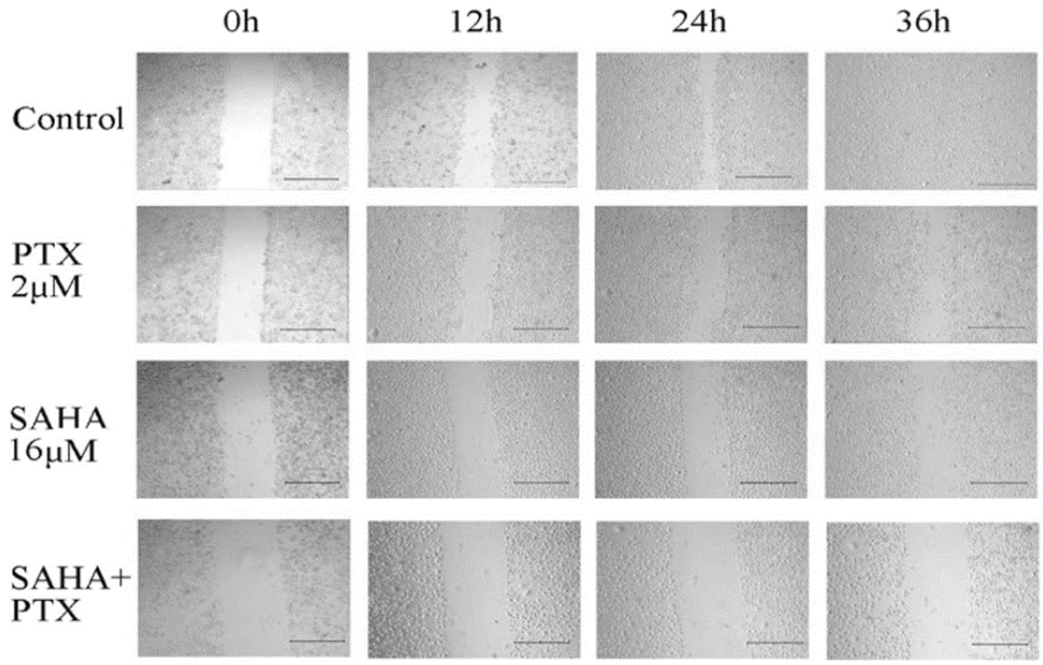

Figure 4. Invasion assay conducted using SAHA, Paclitaxel and SAHA + Paclitaxel combination in a Paclitaxel resistant cell line (scale bar = 100 μm) [15].

The combinatorial treatment using SAHA + Paclitaxel has been evaluated in a few separate clinical trials in other cancer types, including non-small cell lung cancer and recurrent head and neck cancer. A clinical trial assessing the effects of Paclitaxel and carboplatin treatment combined with SAHA or a placebo in advanced non-small cell lung cancer did not find significant differences between the Paclitaxel treatment group and the SAHA + Paclitaxel treatment group, however these patients had also already gone through previous failed chemotherapeutic treatments [18]. While this trial did not find a difference between treatment groups it did demonstrate the safety and minimal side effects in patients. These results in combination with *in vitro* studies demonstrating SAHA reactivity in Paclitaxel resistant EOC patient derived cells

suggests that further studies into SAHA as an EOC therapeutic augmentation are warranted.

Some studies using SAHA have demonstrated that the drug upregulates E-cadherin expression and decreases vimentin expression which also suggests that SAHA could be used to investigate the role of basement membrane in cancer progression by inducing alterations in phenotype of well characterized epithelial and mesenchymal EOC cell lines, however this phenomena is cell and context dependent [13]. In EOC as well as other cancers, progression can be linked to a transition from epithelial to mesenchymal phenotype (EMT) in which localized epithelial cancer cells gain motility, invasiveness, and ability to metastasize (Figure 5). EMT is thought to be involved in the progression of many types of cancer and it involves a weakening of cell-cell and cell-ECM attachments. Clumped aggregates of a mixture of mesenchymal, epithelial and intermediate cells must then survive without anchorage until they reach a new location where they can undergo mesenchymal-epithelial transition (MET) to reverse the process and colonize a new site [19]–[21]. EMT is an integral step in ovulation therefore it is possible that ovarian cells retain this ability which could contribute to the high rates of metastasis seen in EOC patients. Several genes have been linked to the EMT process however the key markers that are widely used to characterize cells are vimentin, an intermediate-filament that is known to be highly expressed in mesenchymal cells, and E-cadherin, a cell adhesion molecule that is a part of the plasma membrane in most epithelial cells [20]–[22]. Although there are several 3D methods for *in vitro* modeling of EOC they do provide a means to capture changes in phenotype related to EMT/MET.

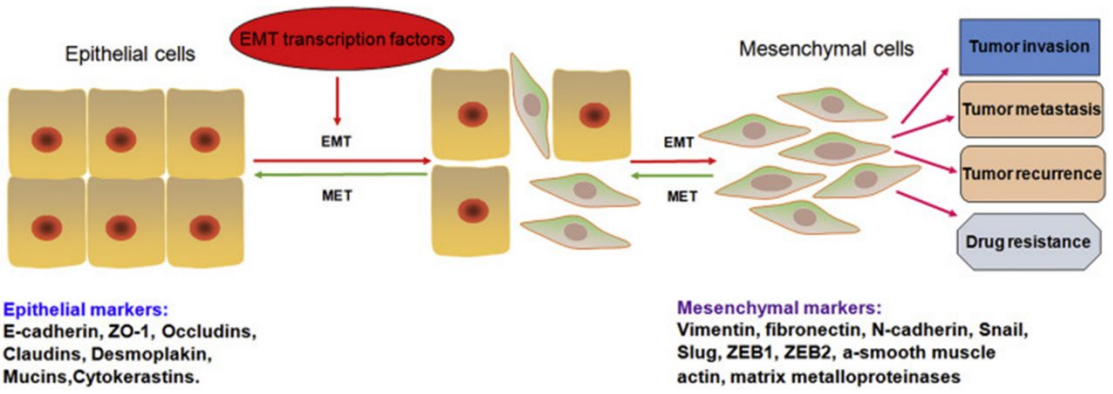

Figure 5. Schematic of the Epithelial to Mesenchymal Transition (EMT) and Mesenchymal to Epithelial Transition (MET) and the implications this process has for cancer progression and metastasis.

While traditional cellular studies using two-dimensional (2D) monolayer cultures have provided a basic understanding of cellular behavior, research over the past several decades has focused on improving the accuracy of *in vitro* models [23]. The importance of three-dimensional (3D) models in cancer research has been recognized as essential in order to mimic the natural tumor microenvironment that is present *in vivo* and the use of spheroids in cancer biology research has become common practice [24]–[26]. There are now several commercially available 3D models for cancer research that facilitate the culturing of cancer cell aggregates and spheroids. Two major categories of 3D culture systems include scaffold and scaffold-free systems [27] (Figure 6). Scaffold free systems rely on the suspension of cells in media in order to form multi-cellular aggregates. These systems include ultra-low attachment plates, hanging drops, and rotating bioreactors or magnetic bead suspension. While scaffold-free platforms do achieve 3D cultured aggregates, they are limited by the fact that they do not lend structural stability to aggregates, they do not provide simple handling of spheroids downstream, and they cannot maintain cultures over extended periods that may be necessary for long term studies. In contrast, scaffold-based culturing systems take

advantage of naturally derived or synthetic hydrogels to provide structural support to aggregates. Although scaffold-based platforms do improve viability and length of culturing, limitations for these platforms include batch to batch variation and the need for additional crosslinking or other structural modifications to encourage cell adhesion. While *in vitro* models enable researchers to probe the dynamics of cancers more deeply, the current commercial 3D culturing platforms are limited in their functionality and the types of studies that they can facilitate.

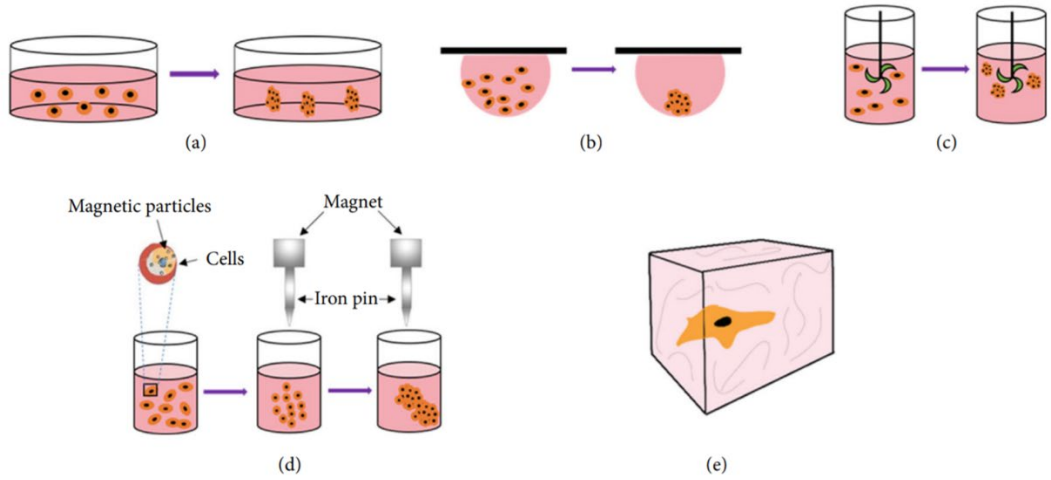

Figure 6. Commercially available 3D culturing systems [27]. (A) Ultra Low Attachment plate. (B) Hanging Drop. (C) Rotating Bioreactor. (D) Magnetic suspension. (E) Hydrogels.

Our lab has developed a novel silicon titanium diboride (Si-TiB_2) micropatterned substrate fabricated using photolithography to deposit TiB_2 micropatterns onto a Si wafer, that has previously been validated for 3D culture of cells from mesenchymal lineage. This substrate addresses the limitations of some conventional commercially available 3D culturing systems. Our platform has previously been validated with both human umbilical vein endothelial cells (HUVECs) and mesenchymal stem cells (MSCs). Furthermore, the Si-TiB_2 platform does not require any pretreatment or coating to facilitate cellular attachment and encourages cells to

deposit their own extracellular matrix proteins, possibly capturing more accurately the relationship between EOC progression and ECM formation.

This study will evaluate the potential of the Si-TiB_2 micropatterned substrate to study the response of EOC to epigenetic and chemotherapeutic drugs. The Si-TiB_2 platform enables immunofluorescent and reflective light imaging of multi-cellular aggregates without the need for complex gel embedding techniques, facilitating the characterization of epithelial and mesenchymal phenotype throughout the metastatic progression.

1.2 Objectives

The overall goal of this study is to evaluate the utility of the Si-TiB_2 micropatterned 3D culturing system in the testing of cancer therapies as well as monitoring phenotypic changes that occur during drug treatment and EMT induction. Study objectives include,

- Comparison of the growth of epithelial (OVCAR3) and intermediate-mesenchymal (SKOV3) cell lines on Si-TiB_2 substrate.
- Investigation of the expression of epithelial and mesenchymal markers on SKOV3 aggregates and OVCAR3 monolayers on Si-TiB_2 substrates throughout culturing periods, ranging from one to two weeks.
- Assessment of effects of epigenetic and chemotherapeutic drugs on epithelial and mesenchymal marker expression in SKOV3 aggregates and OVCAR3 monolayers.

Chapter 2 Materials and Methods

2.1 Micropatterned Substrate Fabrication

Si-TiB2 substrates were fabricated at the University of Houston, Department of Electrical and Computer Engineering, using techniques in the fabrication of integrated circuits. Silicon wafers were used as substrates for deposition of TiB_2 thin films. The phase diagram of TiB_2 allowed for congruent evaporation which ensured well controlled stochiometric composition of the deposited films. The deposition process was done by electron-beam evaporation performed at below 3x10-6 torr pressure from TiB2 chunks. Next, optical lithography using Kasper contact printer was used to create desired patterns in the TiB_2 layers. We used negative photoresist from Futurrex for exposure of the patterns through chromium masks. After the development process of photoresist, the patterns were etched in 30% hydrogen peroxide, washed in acetone for resist removal which was followed by IPA and DI rinse for surface cleaning of the wafers. The TiB2 patterns had circular designs of varying diameters.

2.2 Surface characterization of Micropatterned Substrates and Protein Deposition

Stereomicroscopy images of Si, Si-TiB_2 unpatterned and Si-TiB_2 patterned substrates with circles of varying size from 200 to 500 μm are shown in Figure 7. TiB_2 has greater stiffness, hardness, wettability and roughness as well as less negative charge than the Si background thus facilitating cellular patterning applications. In previous studies, we have demonstrated that the Si-TiB_2 micropatterned substrates promote specific cell adhesion and growth through substrate mediated protein adsorption [28]. Surface roughness is a relatively simple way to control cell adhesion and proliferation,

as studies have shown that increased surface roughness increases these parameters [29], [30]. In previous work we measured the roughness (Rq) of Si at 0.16 nm, while the average Rq of TiB_2 was 0.28 nm [28].

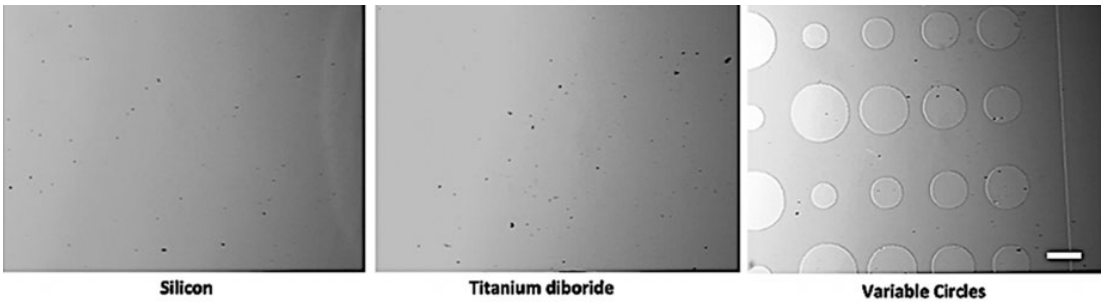

Figure 7. Stereomicroscopy images of Si, TiB_2, and Si-TiB_2 micropatterned substrates taken at 2.5x. (scale bar = 200 μm)

Another vital component of this culturing system is growth factors with a heparin binding domain in combination with heparin. When cells are seeded on Si-TiB_2 micropatterned substrates in the absence of these components the cells demonstrate preferential attachment to TiB_2 patterns vs Si patterns, however when seeded on the same substrates in media supplemented with heparin and growth factors with heparin binding domains, a highly selective attachment to patterns is observed. This is consistent with previous work demonstrating that the 1% heparin as a media component for when culturing on the Si-TiB_2 substrate facilitates selective deposition of Endothelial Cell Growth Supplement (ECGS) onto the TiB_2 micropatterns [28]. Qualitative AFM images of Si only and unpatterned Si-TiB_2 substrates incubated overnight in media with FGF2 in the presence and absence of heparin show relatively equal protein adsorption when heparin is absent. However, when heparin is present protein adsorption is relatively greater on TiB_2 than on Si.

Selective cell adhesion using this system is not limited to a single growth factor, in fact any growth factor with a heparin binding domain is suitable for facilitating TiB_2 pattern-specific growth and aggregation [28]. One possible growth factor to be paired with heparin is fibroblast growth factor (FGF2), which is involved in focal adhesion, chemotaxis in addition to stimulation of cell proliferation. FGF2 is known to be involved in cell adhesion properties and cell-cell communication [31]–[34]. In this study, we use heparin in conjunction with FGF2 to enable micropattern specificity in ovarian cancer cell culture. As determined from previous work in which Atomic Force Microscopy (AFM) was used to determine protein deposition [35], there does not appear to be significant differences in protein adsorption on substrates in media with an FGF2 concentration of 10, 50 or 500 ng/mL. Additionally, previous work using AFM to visualize protein deposition was conducted after incubating clean substrates overnight in media supplemented with 10 ng/mL and 1% heparin (by volume) [35]. Therefore, we utilized a concentration of 10 ng/mL FGF2 in conjunction with 1% heparin.

AFM is a form of high-resolution line scanning probe microscopy that can detect nanoscale differences in surface topography [36]. In previous work Si, Si-TiB_2 unpatterned and Si-TiB_2 patterned substrates were scanned using AFM to assess surface roughness, topography and protein deposition after incubation in media supplemented with 10 ng/mL FGF2 alone and with 1% heparin. The unpatterned Si-TiB_2 substrate in media with FGF2 alone had a higher protein deposition than the unpatterned Si-TiB_2 substrate with FGF2 and heparin. The protein deposition on the Si substrate showed similar results, however the decrease in protein deposition in the presence of both heparin and FGF2 was more significant than that of the TiB_2 substrate. Additionally, the

protein deposition on Si-TiB_2 substrates was relatively uniform while on the Si substrate it was randomly clumped. These results confirm that heparin facilitates differential protein deposition on Si versus micropatterns of TiB_2 on Si. The AFM results demonstrate that heparin decreases the adhesion of proteins on the Si background but not on TiB_2 patterns, suggesting that heparin is involved in binding interactions with growth factors. This is consistent with heparin's involvement in the induction of FGF2 receptor binding [31].

2.3 Cutting and Cleaning of Substrate

Substrates were cut into small squares using a diamond tipped glass scorer and a glass cutting clamp. The surface area of substrates typically ranged from 10 to 20 mm^2. Before seeding of cells, substrates were cleaned using a sonication system for 3-5 minutes first in acetone, then in isopropyl alcohol and finally in deionized water. After each sonication the substrates were scrubbed using a cotton swab before the liquid was aspirated and the substrates were transferred into the next cleaning solution. The substrates were then dried using a pressurized nitrogen air gun before placing one substrate per well into a 24-well plate. The types of substrates used in this study included silicon (Si) only, unpatterned titanium on Si and micropatterned Si-TiB_2. The micropatterned Si-TiB_2 substrates consisted of patterns ranging from a diameter of 200 μm to 500 μm in increments of 50 μm, for a total of 7 different circle sizes.

2.4 SKOV3 and OVCAR3 Passaging and Seeding

SKOV3 and OVCAR3 cell lines were maintained in 2D cultures in 5 mL of cancer media (CM) in 25 mL flasks and passaged when they reached approximately

80% confluency into new flasks. Incubator conditions were humidified, 5% CO_2 and 37°C. Cancer media was composed of 20% fetal bovine serum (FBS) (12306C Millipore Sigma), 1% antibiotics (Sigma-Aldrich A5955), and 0.1% insulin (ABM TM053) in RPMI 1640 with glutamine (02-0205 VWR Life Science). For passaging, CM was aspirated and cells in flasks were washed twice with 2.5 mL 1X phosphate buffered saline (PBS) (Sigma-Aldrich H6648). PBS was then aspirated, and cells were incubated in 2.5 mL of 0.05% 1 mM trypsin from bovine pancreas (Sigma-Aldrich 59417) in the humidified incubator for 3-5 minutes. After incubation in trypsin cell detachment was verified with a phase contrast microscope and 2.5 mL of CM was added to the flask to deactivate trypsin. The 5mL of solution was transferred from the flask to a 15 mL centrifuge tube for centrifugation at 800 x g for 3-4 minutes in order to pellet cells. Supernatant was aspirated and cells were resuspended in 1 mL of fresh CM. Cells were counted in a hemocytometer by adding 12 µL cell suspension. A new culture flask was plated typically with 5 mL of CM and 250,000 cells from the cell suspension, however the number of cells plated was adjusted to achieve confluency earlier or later as needed.

During the same passages, substrates would also be seeded. After determining the cells count, the suspension was concentrated or diluted to achieve a final concentration of 1200 cells/µL. Substrates that had previously been cut, cleaned and imaged to determine surface area were placed one per well into a 24-well plate. These substrates were seeded using the prepared cell suspension based on their surface area (volume = ½ surface area of substrate) to a final seeding density of 600 cells per μm^2. Next, 1 mL of culture media (CM supplemented with 10 ng/mL human FGF2 (Sigma-Aldrich F0291) and 1% heparin (Sigma-Aldrich H3393)) was then added to each of the

wells by allowing the media to gently flow down the wall of the well in order to minimize disturbance of cells on the substrate. The freshly seeded substrates were carefully transferred to a humidified incubator 37°C with 5% CO_2. Every 48 hours the old culture media was aspirated, and 1 mL of fresh culture media was added.

Seeding of hanging drop aggregates used the same concentration of cells in suspension as the substrates, therefore the passaging and resuspension protocols were the same however the media that was used for resuspension was the supplemented culture media rather than CM. 100 mL petri dishes were filled with PBS to cover the bottom. The lid of the dish was inverted and 10 μL droplets of cell suspension were deposited on its' surface. The lid was carefully flipped upright to not disturb the droplets and placed over the PBS filled bottom. The petri dish was carefully transferred to the incubator. Every 48 hours the petri dish lid was inverted, and the old culture media was carefully removed using a micropipette before 10 μL fresh culture media was added.

2.5 Stereomicroscopy

After substrates were cleaned, they were imaged using an Olympus S2X7 Microscope at 1x resolution. This image was used to calculate the surface area of the substrate by using the free form select tool to sketch around the edges of the substrate and calculate the enclosed surface area based on known dimensions of pixel count per mm. These surface area measurements were used to calculate the amount of cell suspension needed to seed the substrates at an appropriate density. Additionally, 1-4 quadrants of the substrates (based on substrate size) were imaged at 2.5x resolution to capture initial images before cell culturing to assess longitudinal cell growth. During experiments, the substrate quadrants were imaged at 2.5x resolution every 48 hours to

capture cellular growth on substrates by transferring the substrates to a 35 mL petri dish with supplemented CM.

2.6 Drug Treatment

2.6.1 SAHA drug treatment

A stock solution of SAHA (Cayman Chemical Company #10009929) was prepared at a concentration of 1000 μM in DMSO (Sigma-Aldrich D8418). To treat the cells on substrates the SAHA was diluted in supplemented CM to a final sublethal dosage of 3 μM [35], [37]–[39].

2.6.2 Paclitaxel drug treatment

Paclitaxel (Cayman Chemical Company, 33069-62-4) was prepared in a stock solution of 1000 μM in DMSO. To treat the cells on substrates, the Paclitaxel stock solution was diluted in supplemented CM to a final sublethal dosage of 0.05 μM [16], [40], [41].

2.7 Viability Protocol

To assess viability, substrates were transferred to a 35 mL petri dish with 2 mL 1X PBS, 0.5 μL 10 mg/mL Acridine Orange (AO, Biotium 40039), 0.5 μL 1 mg/mL Propidium Iodine (PI, Biotium 40017) and 5 μM DAPI. The substrates were left to incubate in the dark for 30 minutes before imaging with a confocal microscope (excitations for AO, PI and DAPI were 488 nm, 533 nm and 405 nm respectively). Image analysis was conducted in Fiji/ImageJ using a custom written macro software to calculate the percent of viable cells and dead cells in the TiB_2 patterns.

2.8 Immunofluorescent Histochemistry Staining Protocol

To assess and monitor phenotype of cultured cells, substrates were first rinsed gently by transferring them to a 35 mL petri dish containing 2 mL 1X PBS twice, followed by a 15-minutes incubation in 4% paraformaldehyde (Electron Microscopy Science, 15710) in 1X PBS for cell fixation. Then the substrates were washed by gently transferring them again in 2 mL of 1X PBS in a 35 mL petri dish. Cells were then blocked in 5% donkey serum in 0.15% Triton-X 100 (Jackson ImmunoResearch Laboratories 017-000-121) in 1X PBS either for 1 hour at room temperature or overnight at 4 degrees Celsius. After blocking, the cells were gently washed twice in 0.2% Triton-X 100 in 1X PBS in 35 mL petri dishes. After this the prepared fixed and blocked cells on substrates were ready to be stained or stored in 1X PBS at 4 degrees Celsius.

To conduct staining, the cells were first washed in 0.2% Triton-X 100 in 1X PBS before incubation in primary antibodies by depositing 50 μL of prepared antibody solution onto a 100 mL petri dish lined with parafilm and depositing a substrate into the droplet. Antibodies were diluted in 0.15% Triton-X 100 and 1% BSA in 1X PBS. The substrates were then covered and left either at room temperature for one hour or overnight at 4 degrees Celsius. Primary antibodies used in this study include anti-vimentin (1:100, rabbit monoclonal anti-vimentin, Abcam, ab16700) and anti-Ki67 (1:100, mouse monoclonal anti-Ki67, Santa Cruz Biotechnology, sc-2390).

Next, substrates were washed twice in 0.2% Triton-X 100 in 1X PBS and then incubated in secondary antibodies prepared in 0.15% Triton-X 100 and 1% BSA in 1X PBS. The prepared antibody solutions were deposited in the same manner as the primary

antibodies and the substrates were placed in the droplets. They were again left to incubate for 1 hour at room temperature or overnight at 4 degrees Celsius, covered in foil to prevent antibody degradation due to the light sensitivity of the secondary antibodies. Secondary antibodies were all purchased from Jackson ImmunoResearch Laboratories and included Alexa-Fluor 647-AffiniPure Goat Anti-Mouse (1:500, excitation 647 nm) , Alexa-Fluor 594-AffiniPure Donkey Anti-Rabbit (1:500, excitation 594 nm) and Phalloidin-iFluor 488 reagent ab176753 (1:1000, excitation 488 nm). After the secondary antibody incubation, substrates were washed twice in 0.2% Triton-X 100 in 1X PBS before being placed in 2 mL 1X PBS with 10 μL of 0.02 mg/mL DAPI (Biotium, 40043) and allowed to incubate covered in foil for 15 minutes before imaging. To prepare substrates for imaging they were transferred to glass microscope slides and a single droplet of VectaSheild Antifade Mounting Medium (H-1700 Vector Laboratories) was dropped on top of each substrate.

Substrates were imaged on an Olympus Fluoview 1000 Confocal Microscope at 4x and 20x magnification. For each set of conditions, a minimum of 3 separate experiments were conducted and from each trial at least one substrate was stained and a minimum of 3 patterns of varying sizes (200, 250, 300, 350, 400, 450, 500 μm) were imaged.

2.9 RT qPCR Protocol

Analysis of aggregates at desired time points using RT qPCR was performed by first gently washing substrates in 1X PBS and then 2 mL 0.05% trypsin from bovine pancreas (Sigma-Aldrich 59417) for 4 minutes in the incubator at 35 degrees Celsius and 5% CO_2. Trypsin was neutralized with 2 mL culture media before disturbing the

aggregates with the tip of a micropipette until all cells were loosened. The media with cells was then centrifuged to form a pellet at 4,000 x g before being resuspended in 1 mL 1X PBS and spun down again at 4000 x g and 4 degrees Celsius and discarding supernatant. At this stage samples could be stored at -80 degrees Celsius for later processing.

Next, RNA was extracted from the sample using the PureLink ® RNA Mini Kit (Thermo Fischer Scientific, 12183025) and accompanying protocol. Briefly, the cell pellet was resuspended in 0.3 mL of Lysis buffer prepared with 2-mercaptoethanol and then vortexed. Homogenization was performed using an 18-20 gauge needle, passing the lysate up and down 5 times. Once lysate was homogenized 0.3 mL 70% ethanol was added to each sample and vortexed before transferring the sample to a spin cartridge and centrifugation at 12,000 x g for 15-30 seconds. Flowthrough was discarded and cartridge was washed with 700 µL Wash Buffer I and then twice in 500 µL Wash Buffer II spinning down at 12,000 x g and discarding flow through each time. Spin cartridge was then dried by spinning at 12,000 x g for 1 minute before transferring the cartridge to a recovery tube. The membrane bound RNA was extracted by adding 20 µL RNase-free water to the center of the spin cartridge. Membrane was allowed to incubate at room temperature for 1 minute before eluting the extracted RNA at 12,000 x g for 2 minutes. RNA concentrations (ng/µL) were determined using a Nanodrop 1000 (Thermo Scientific). At this point the samples could then be stored at -80 degrees Celsius before further processing.

To prepare cDNA from RNA samples, the iScript ™ cDNA synthesis Kit was used (Bio-Rad, 1078891). Briefly, RNA concentration of each sample was used to

determine the volume of sample that would contain 0.1 µg of RNA. This sample volume was added to a reaction tube along with 4 µL of 5x iScript Reaction mix, 1 µL iScript Reverse Transcriptase and enough nuclease free water to reach a final volume of 20 µL for each sample. Samples were then placed in a thermocycler that performed priming at 25 degrees Celsius for 5 minutes, reverse transcription at 46 degrees Celsius for 20 minutes and RT inactivation at 96 degrees Celsius for 1 minute. After cDNA synthesis samples were then stored at -80 degrees Celsius until it was time to run RT qPCR.

To run the qPCR, cDNA from samples was first diluted at 1:10 in Nuclease free water. Forward and reverse primers for each gene of interest were prepared at a concentration of 10 µM and a then used to prepare the reaction mix which included per well included 5 µL SYBR Green, 2.6 µL nuclease free water and 0.2 µL of both the forward and reverse primers for the gene of interest. The total volume of reaction mix for each well of the 96 well qPCR plate was 10 µL which included 8 µL of reaction mix and 2 µL of sample cDNA dilution. The Plate was placed in a thermocycler for 40 cycles which consisted of 1 minute 15 seconds at 95 degrees Celsius, 30 seconds at 60 degrees Celsius, 15 seconds at 95 degrees Celsius, and 1 minute at 60 degrees Celsius.

2.10 Statistical Analysis

Analysis of confocal images was conducted using a macro designed to be compatible with Fiji in ImageJ. This macro determined the percentage of viable cells in the case of AO/PI staining. For antibody stains, the macro computed total pixel count for each of the stains. The macro calculated thickness of the aggregates using the coordinates of the z slices of the images and manual selection of the aggregate boundaries enabled the calculation of the aggregate's diameter. Overall viability was

calculated by a percentage of the AO to PI staining. Relative expression of a given marker was calculated in excel by normalizing the pixels of a marker to the pixels of DAPI in an aggregate.

Statistical analysis of data from the macro was conducted in excel using PHStat. To compare two data sets the Student's T-test while comparisons across more than two data sets were conducted using ANOVA and Turkey-Kramer tests. Significance was assumed to be $p < 0.05$.

Data from qPCR was analyzed in excel using template to analyze the CT values and determine fold change. Comparisons were made to a house keeping gene GAPDH.

Chapter 3 Results

3.1 Growth of SKOV3 and OVCAR3 on Micropatterned Substrates

Previous studies have demonstrated that the Si-TiB_2 micropatterned substrates are useful in culturing mesenchymal stem cells [28]. The Si-TiB_2 micropatterned substrate was shown to support patterned cell organization and growth for two EOC cell lines, SKOV3 and OVCAR3.

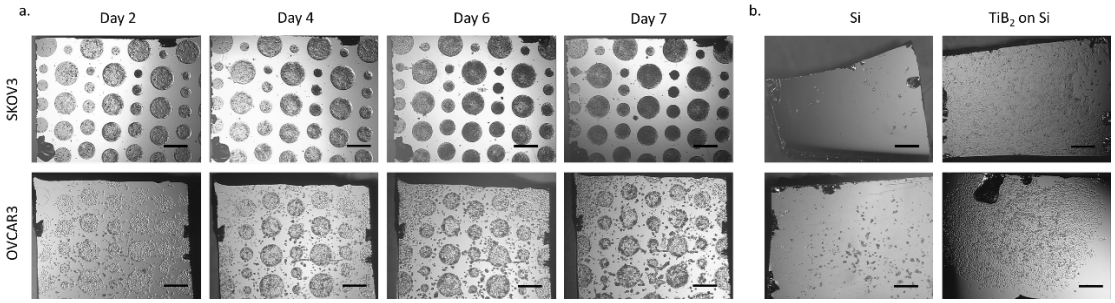

Figure 8. Representative images of SKOV3 and OVCAR3 cultured on Si-TiB_2 substrates (scale bar = 500 μm). (A) SKOV3 and OVCAR3 on Si-TiB_2 with circle patterns ranging from 200-500 μm over a 7-day period. (B) SKOV3 and OVCAR3 on Si only and unpatterned Si-TiB_2 on day 2.

SKOV3 and OVCAR3 cells were grown on the Si-TiB_2 micropatterned substrate over one week and monitored using stereomicroscope imaging every 48 hours.

Representative images of these one-week cultures are shown in Figure 8a. While OVCAR3 cells maintained relatively specific monolayer growth on the TiB_2 circular patterns with some cell growth on the Si background as the days progressed, SKOV3 cells demonstrated highly specific growth in the TiB_2 circular patterns and spontaneously formed 3D aggregates.

Additionally, attempts to culture OVCAR3 and SKOV3 on Si only substrates demonstrates that both cell lines struggle to maintain adhesion to Si substrates, while they adhere and proliferate rapidly on the TiB_2 substrates (Figure 8).

Staining of SKOV3 and OVCAR3 cells on day 7 of culture on Si-TiB_2 micropatterned substrates with F-actin further reveals the differences in structure between the SKOV3 aggregates and the OVCAR3 monolayers. As seen in Figure 9 imaging SKOV3 aggregates with a confocal laser microscope requires several slices, meanwhile OVCAR3 monolayers can be captured with less than half the number of image slices. Additionally, F-actin staining reveals how densely packed the SKOV3 aggregates are compared to the OVCAR3 monolayers.

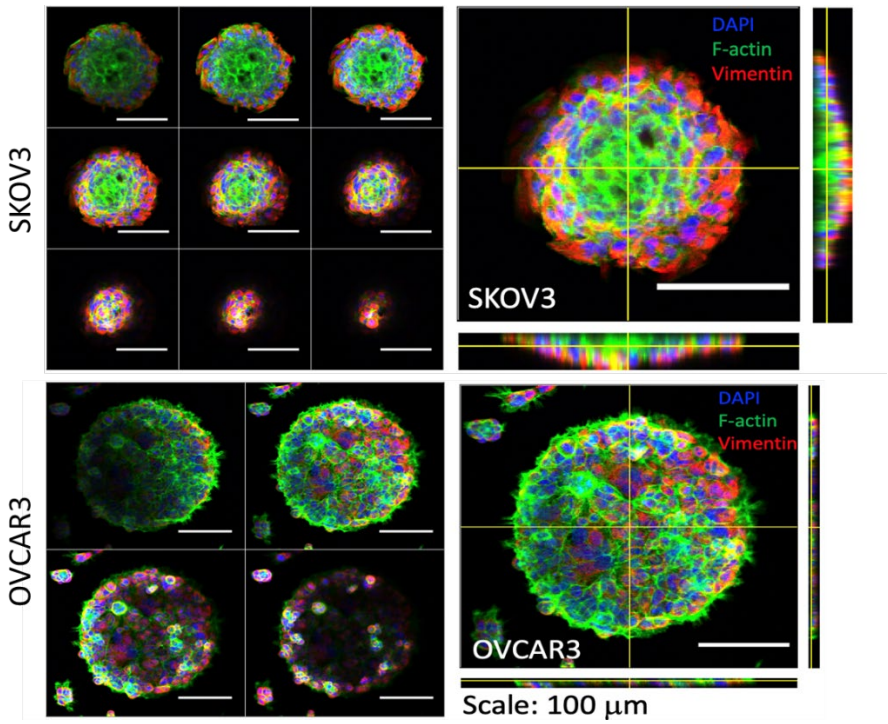

Figure 9. Representative Immunofluorescent images of SKOV3 and OVCAR3 on day 7 of culture with DAPI (blue), F-actin (green) and vimentin (red) (scale bar = 100 µm).

3.1.1 Comparison to Other Platforms

Figure 10 shows spheroids generated using hanging drop method that demonstrate similar results, where OVCAR3 yields loose, poorly defined aggregates while SKOV3 yields tightly formed aggregates. These findings are similar to those in studies using suspension methods, where they demonstrate that epithelial OVCAR3 forms relatively loose aggregates or monolayers [42], [43]. However, the study by Sodek et al found that the hanging drop method yielded loose aggregates from SKOV3 cells as well, while our use of the hanging drop method as well as Si-TiB_2 platform shows strong aggregation.

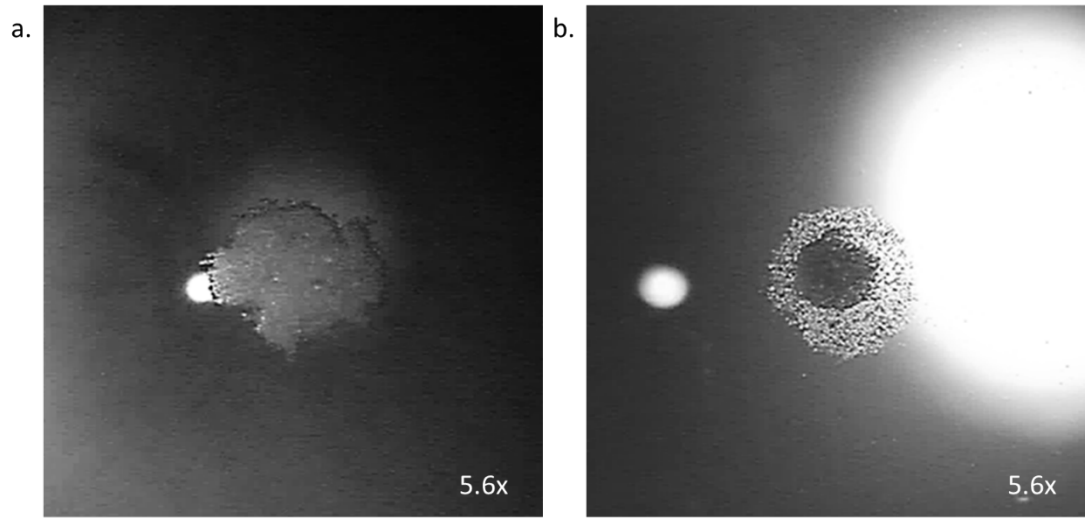

Figure 10. Representative images of EOC hanging drop cultures on day 8 (scale = 5.6x zoom). (A) OVCAR3 (B) SKOV3

Another commercially available 3D culturing system, the Ultra Low Attachment Plate (ULP) system was used to assess how our Si-TiB_2 platform compared. In order to determine whether our platform maintained SKOV3 in its mesenchymal phenotype, ULPs were used to culture SKOV3 cells for 7 days and then sampled for qPCR analysis of mesenchymal (MMP2 and vimentin) and epithelial (Claudin-8 and E-cadherin) gene expression) (Figure 11). SKOV3 cells cultured on the Si-TiB_2 platform showed higher levels of mesenchymal markers and lower levels of epithelial markers, suggesting that ULPs do not maintain SKOV3 in it's mesenchymal state as well as the Si-TiB_2 platform (Figure 11b)

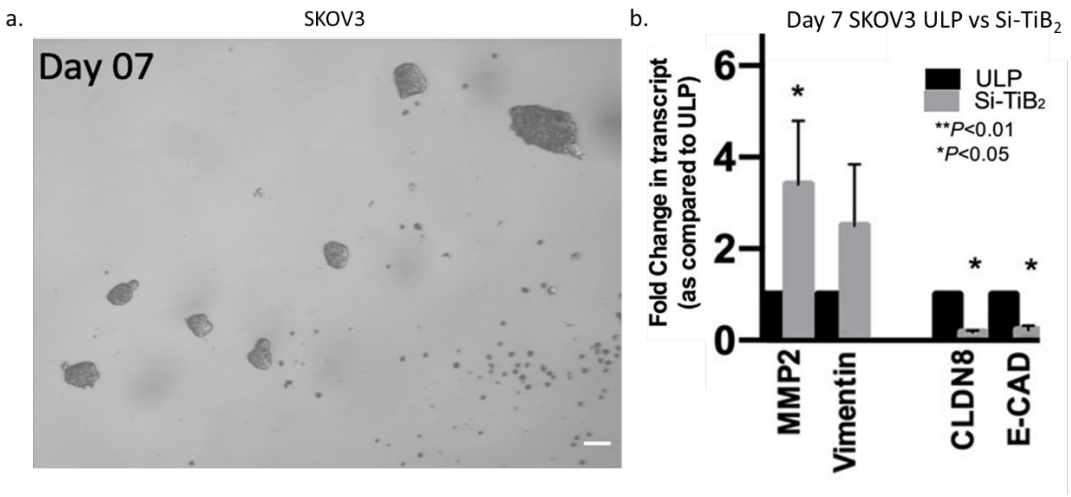

Figure 11. Culturing of SKOV3 cells in Ultra Low Attachment Plates (ULPs) (A) Day 7 representative images of SKOV3 aggregates in ULP culture. (scale bar = 100 μm) (B) Phenotypic analysis of SKOV3 aggregates on Day 7 of culture in ULPs vs Si-TiB_2 micropatterned substrates (qPCR performed in triplicate for each experiment, from n>3 experiments per condition).

3.1.2 Long Term Culture

Long term (2 weeks) growth of OVCAR3 and SKOV3 cells shown in Figure 12 on Si-TiB_2 micropatterned substrates further emphasize this difference, as increase in culture time of SKOV3 cells resulted in larger and tighter aggregates, meanwhile the OVCAR3 cells begin to form a thick monolayer across the entire substrate, regardless of micropattern or background. SKOV3 maintains specificity until day 9, and by day 14 had moved onto the Si background, but still maintained thick aggregation over the patterns.

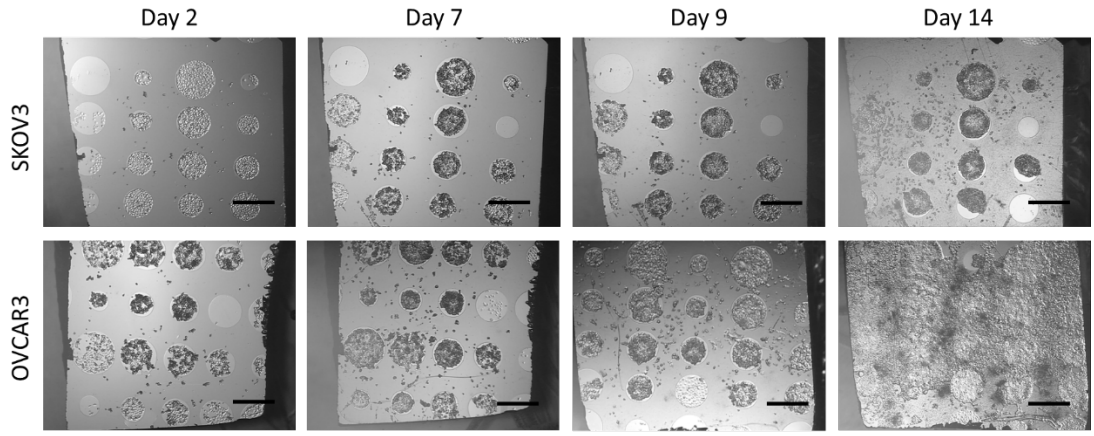

Figure 12. Representative stereomicroscopy images of long-term culturing through day 14 on Si-TiB_2 substrates of SKOV3 and OVCAR3 cells (scale bar = 500 μm).

3.2 SKOV3 3D aggregate and OVCAR3 monolayer Characterization

3.2.1 Dimensions

Characterization of the relationship between pattern size and aggregate diameter and depth was conducted using confocal microscopy images of cells stained with DAPI, F-actin and other markers, results shown in Figure 13 are data collected from previous work along with new data from this study [35], [37]. The SKOV3 results demonstrated that the aggregate diameter was dependent on pattern diameter with the largest aggregate diameters occurring on the largest diameter patterns (N = 11 repeats with a minimum of 1 substrate and maximum of 4 substrates per repeat, resulting in a minimum sampling of 9 aggregates per micropattern size for a total of 79 aggregates, p=0.0000), while an analysis of the thickness of the same aggregate samples was not found to be significantly different based on micropattern size (p=0.3333). The average aggregate thickness was 50.08 μm with a range from 22 to 88 μm. These dimensions correspond with the lower end in size of EOC multicellular spheroids present in peritoneal ascites, which typically range from 50 to 700 μm [42], [44], [45]. Additionally, these

dimensions are similar to those reported in studies using hanging droplets in which ideal diameter and thickness for optimal diffusion of nutrients in compact aggregates is 400 and 100 μm respectively [46].

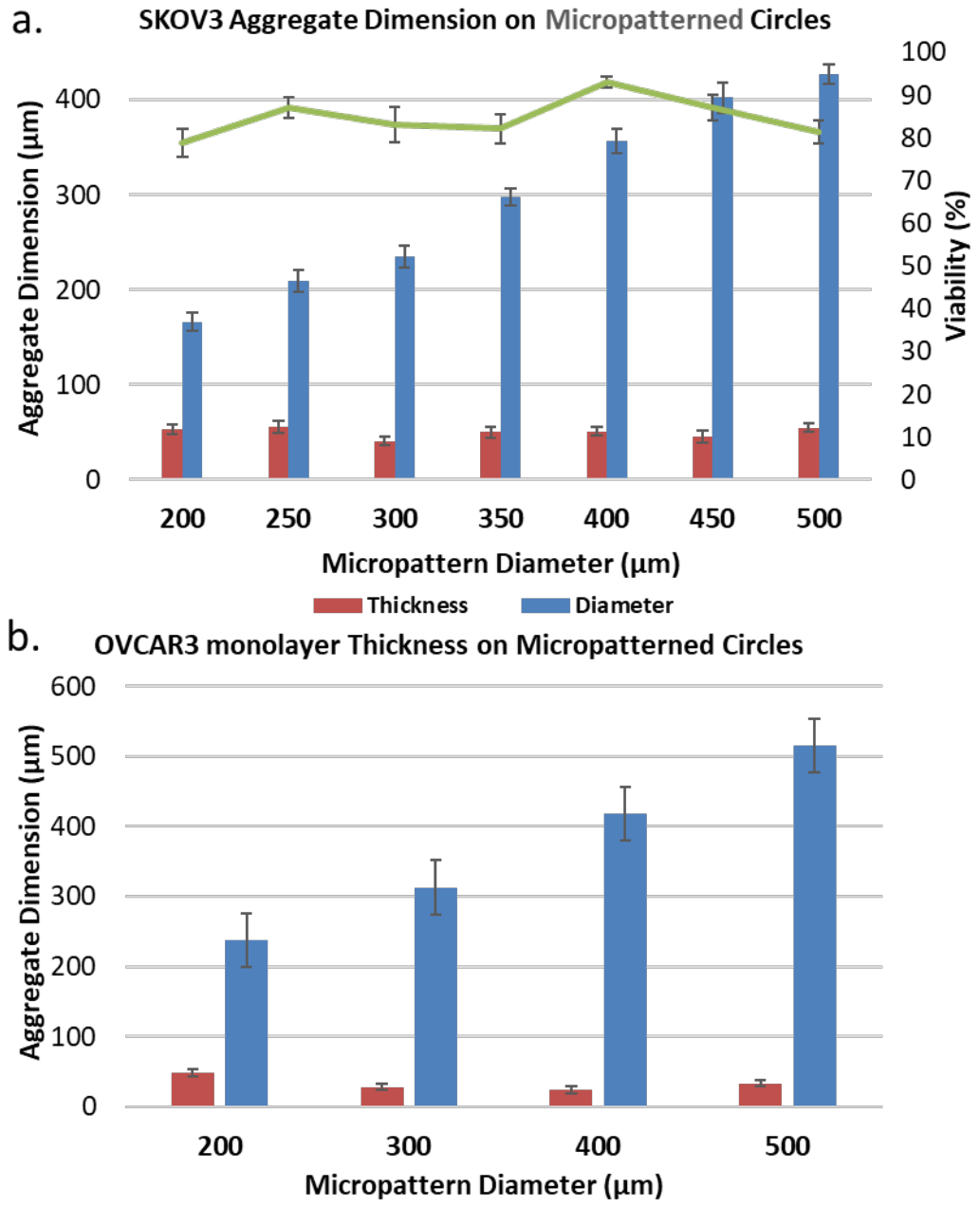

Figure 13. Day 7 mean of dimensions and viability measurements with standard error bars (green=viability) (n>9 for each aggregate size). (A) SKOV3 and (B) OVCAR3.

OVCAR3 culturing on Si-TiB_2 showed similar results, however since they do not form proper aggregates the thickness measured was a thickness of the monolayers growing on the patterns and diameter was the diameter of the monolayer where cells were present (Figure 13).

Additionally, the viability assessments of SKOV3 aggregates on Si-TiB_2 on day 7 were performed using AO/PI staining but such assessments could not be performed on OVCAR3 samples as the cells lost adherence during multiple attempts at viability staining (Figure 13). Although SKOV3 aggregate diameter was dependent on pattern diameter, the viability across all pattern sizes was consistent, with a range of 81-86% and an average viability of 83%. This is consistent with existing studies that report 3D spheroid viability of roughly 80% in SKOV3 spheroids formed via hanging drop method [47].

3.2.2 SKOV3 and OVCAR3 Phenotype and morphology

To determine the morphology and phenotype of OVCAR3 and SKOV3 cells cultured on Si-TiB_2 micropatterned substrates immunofluorescence imaging was used.

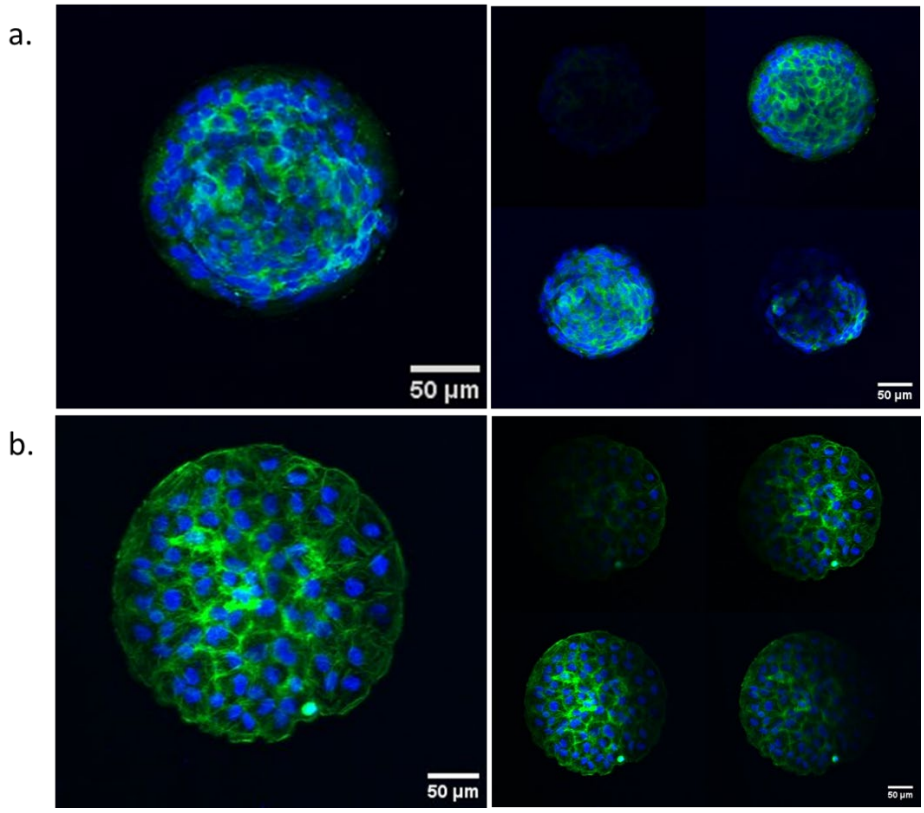

Figure 14. Cytoskeletal morphology visualized via F-actin labeling following 7-day culture on Si-TiB_2 micropatterned substrates (scale bar = 50 µm). (A) SKOV3 (B) OVCAR3

A common morphology marker for mammalian cells is F-Actin, since it is a vital cytoskeletal component, which is important for stability, motility and many cellular functions. As mentioned in Friguglietti et al., F-Actin is capable of capturing the cytoskeleton structure as this stain binds to all types of actin filaments, which make op the cytoskeletal structures of all animal cells. This enables us to discern the spindle like morphology of SKOV3 and the rounded, cobblestone morphology of epithelial cells like OVCAR3, therefore, we used F-actin to capture the morphological differences between the two cell lines. Figure 14 shows the morphology of SKOV3 and OVCAR3 after 7 days of culture on the Si-TiB_2 micropatterned substrates.

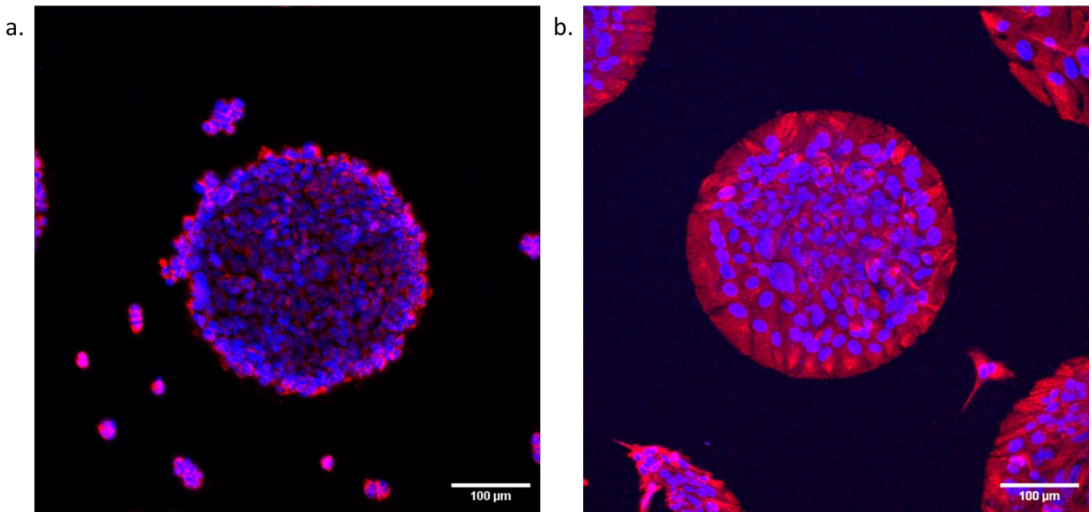

Figure 15. Representative Day 7 images of cells labeled for vimentin and DAPI (scale bar = 100 µm). (A) OVCAR3 (B) SKOV3.

As mentioned previously, the intermediate filament vimentin has been implicated as a mesenchymal cell marker which can be used to assess epithelial cells for mesenchymal properties and is often used to monitor cells expected to be undergoing EMT/MET [3], [22], [48], [49]. We chose to use vimentin as a marker for monitoring the phenotype of the SKOV3 and OVCAR3 cells. Initial images of OVCAR3 and SKOV3 cells before drug treatment on day 5 and 7 respectively show highest concentrations of vimentin along the border of circular patterns where the TiB_2 pattern and Si background meet (Figure 15).

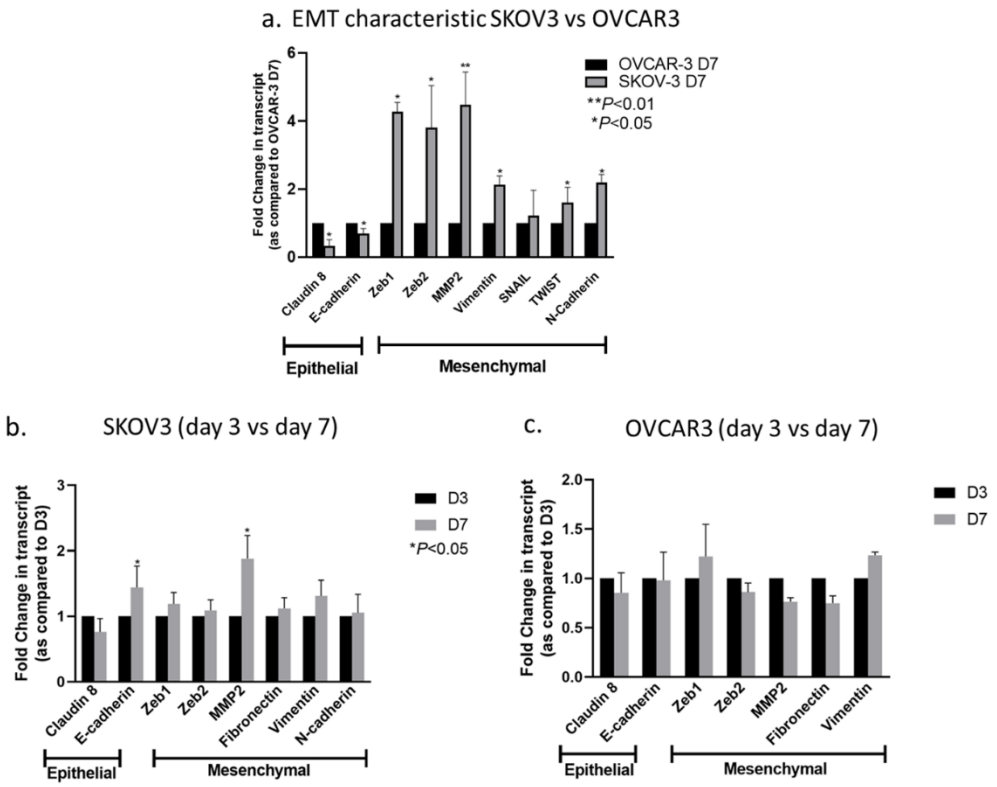

Figure 16. qPCR analysis of epithelial and mesenchymal associated genes in cells cultured on Si-TiB_2 micropatterned substrates (mean expression with standard error bars, qPCR performed in triplicate for each experiment, from n>3 experiments per condition). (A) SKOV3 vs OVCAR3 on day7. (B) SKOV3 day 3 vs day 7. (C) OVCAR3 day 3 vs day 7.

In order to characterize baseline expressions of epithelial and mesenchymal genes in SKOV3 and OVCAR3 cells qPCR was used. These genes include Claudin 8, E-cadherin, Zeb1, Zeb2, MMP2, Fibronectin, vimentin and N-cadherin (Table 1). As shown in Figure 16a, SKOV3 has a more mesenchymal phenotype than OVCAR3. Expression of E-cadherin and MMP2 were significantly upregulated in SKOV3 from day 3 to day 7 however since SKOV3 has an intermediate-mesenchymal phenotype this is not an indication of phenotypic change since MMP2 is a mesenchymal marker and E-cadherin is an epithelial marker (Figure 16b). In OVCAR3 there were no significant changes in expression for any of the genes (Figure 16c).

Table 1. List of genes for qPCR phenotypic analysis and their function

Gene	Function/Role	Association
Claudin 8	integral membrane protein, component oftight junction strands	Epithelial
E-cadherin	membrane protein of epithelial cells	Epithelial
Zeb1	suppressor of epithelial markers, including E-cadherin	Mesenchymal
Zeb2	transcription factor in transforming growth factor β (TGFβ) pathway	Mesenchymal
MMP2	Matrix Metallopeptidase 2, extracellular matrix component	Mesenchymal
Fibronectin	extracellular matrix component	ECM
Vimentin	type III intermediate filament protein present in mesenchymal cells	Mesenchymal

3.2.3 Proliferation in SKOV3 and OVCAR3

A commonly used proliferation marker in tumor growth studies is Ki-67. The expression of Ki-67 is associated with tumor cell proliferation and is also used in clinical pathological assessments of patient biopsies. Studies utilizing 3D cultures to assess drug treatments frequently use Ki-67 to compare expression after treatment to a baseline expression taken before treatment [50]. Therefore, we used Ki-67 to collect a baseline proliferation marker expression on day 7 in SKOV3 and OVCAR3, which demonstrated that after SAHA treatment SKOV3 aggregates significantly reduced in proliferation while OVCAR3 monolayers saw a slight reduction in proliferation but statistical analysis revealed that in OVCAR3 this reduction was not significant (Figure 17).

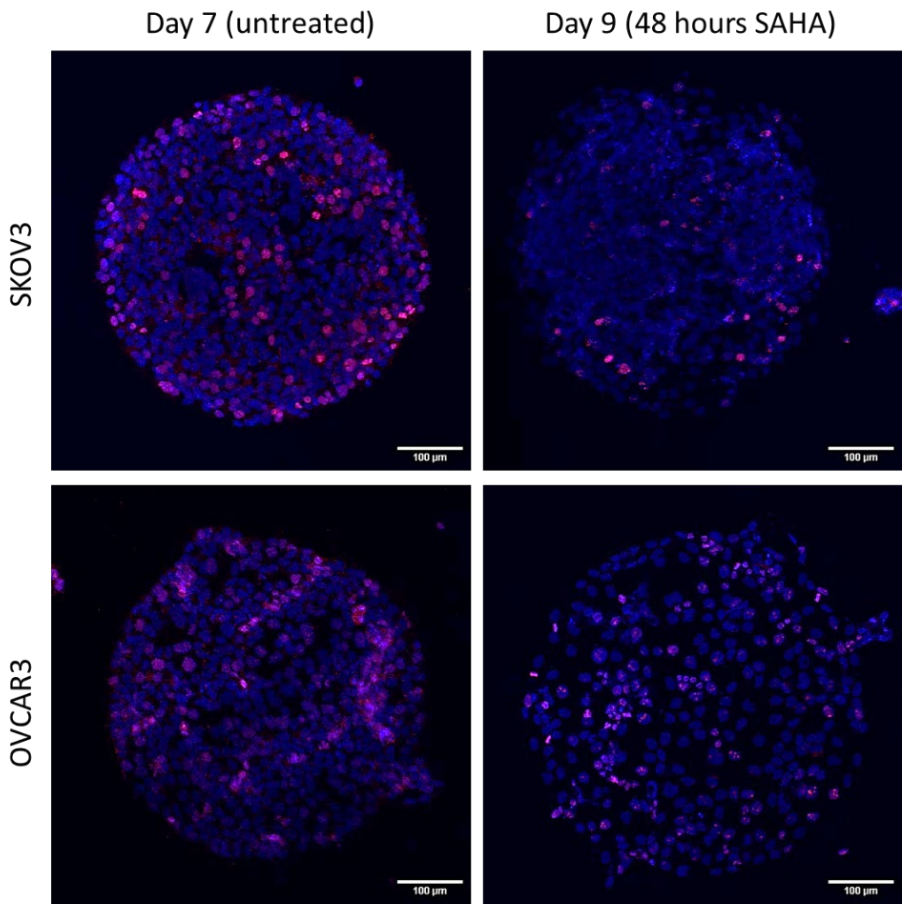

Figure 17. OVCAR3 and SKOV3 cells on Si-TiB_2 micropatterned substrates stained for Ki-67 expression on day 7 before SAHA treatment and day 9, 48 hours after SAHA treatment (scale bar 100 µm).

3.3 Effects of drug treatment on SKOV3 aggregates and OVCAR3 monolayers

3.3.1 SAHA treatment

Previous work demonstrated SAHA's effects on SKOV3 aggregates after 48 hour treatment starting on day 7 with a dose of 3 µM [35], [37]. Combining data from previous studies with that of the current study, we found that there was a reduction in aggregate size 48 hours after SAHA treatment and staining with AO/PI showed that aggregates did not have a significant reduction in viability before versus after SAHA treatment (Figure 18) [35], [37].

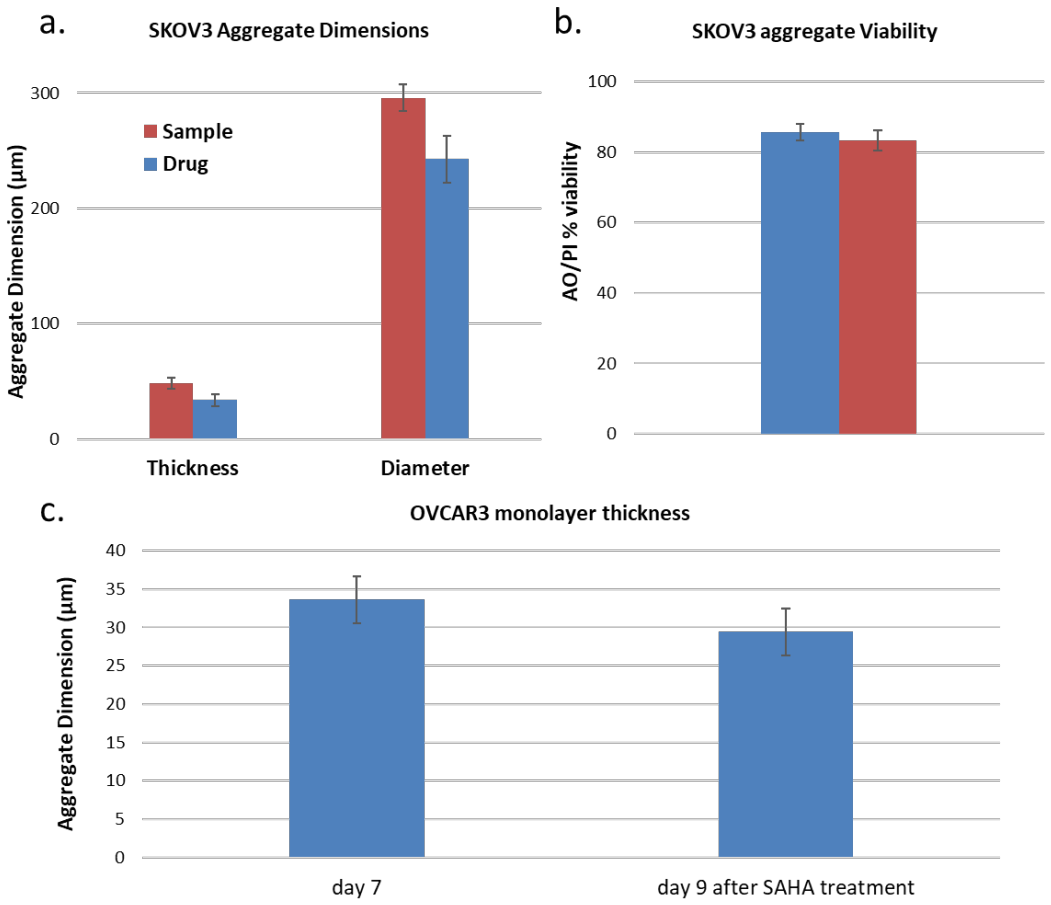

Figure 18. Mean dimensions of cells cultured on Si-TiB_2 aggregates or monolayers before and after SAHA treatment with standard error bars (n>3 replicates, with >3 aggregates sampled per experiment). (A) thickness (p=1.71E-07) and diameter (p=1.07E-15) of SKOV3 aggregates (B) AO/PI viability of SKOV3 aggregates (p=0.2127) (C) thickness of OVCAR3 monolayers (p=0.2607)

Although OVCAR3 does not form proper aggregates on the Si-TiB_2 platform, we decided to carry out the same study with OVCAR3 cells in order to determine if SAHA treatment yields different results depending on phenotype. Representative images of OVCAR3 before and after SAHA treatment, seen in Figure 20, showed a loss of cells on Si and a thinning of OVCAR3 cells monolayers on the TiB_2 patterns. However, analysis of the monolayer thicknesses does not show a statistically significant difference. Additionally, Figure 17 shows representative images of Ki67 before and after SAHA treatment which shows a significant decrease in proliferation in SKOV3

(p= 0.03515) and an insignificant decrease in OVCAR3 (p=0.1835) after SAHA treatment.

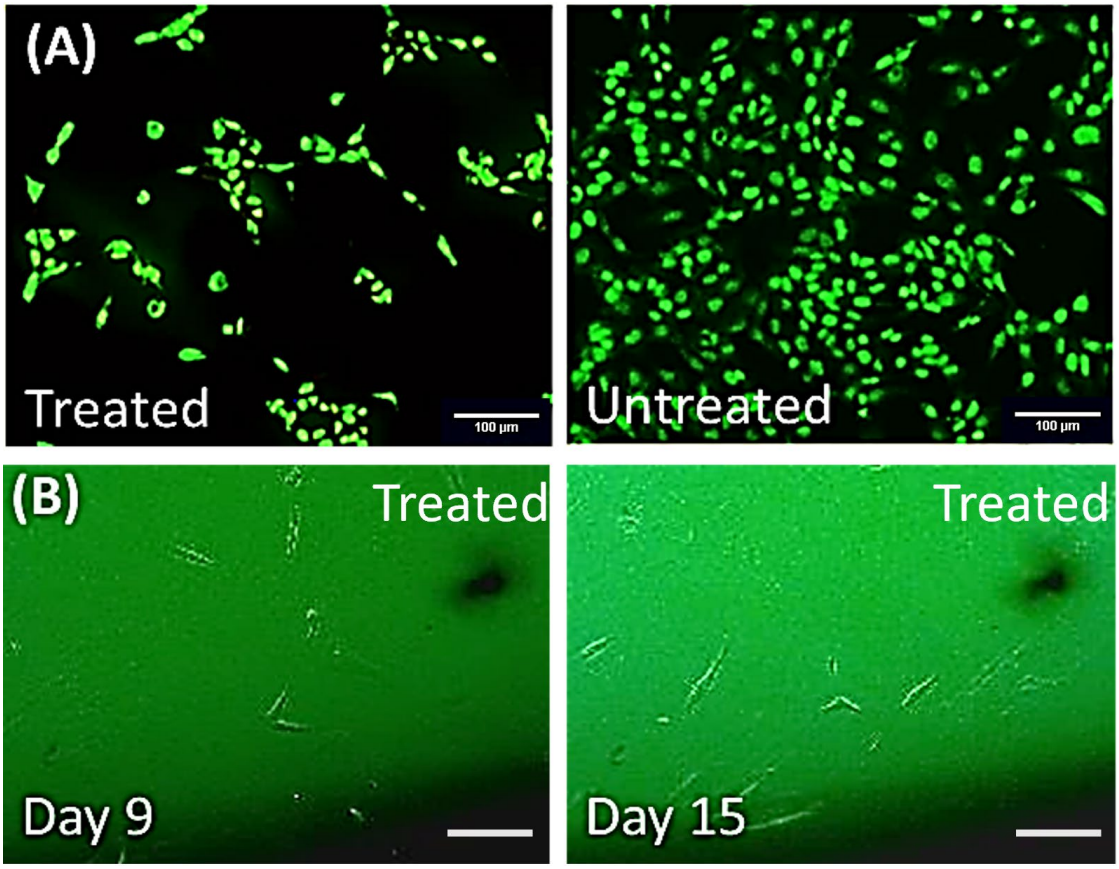

Figure 19. Representative images of disaggregated SKOV3 cells replated before vs. after SAHA treatment. (A) Replated SKOV3 cells stained for viability (AO/PI) that have disaggregated after treatment with SAHA vs those which naturally disaggregate under normal culturing conditions (scale bar = 100 µm). (B) Light microscope images of disaggregates SKOV3 cells after SAHA treatment allowed to culture for 9 and 15 days (scale bar = 100 µm).

To determine the fate of cells that have been disaggregated by SAHA treatment, loose cells in the surrounding media after 48 hours of SAHA treatment were collected and reseeded in MayTek wells. These cells were assessed for viability and allowed to culture for 15 days. As seen in Figure 19, disaggregated cells remained

viable however they did not proliferate very much. Very little increase in cells on the MayTek dish was seen even after 15 days of culture in untreated media.

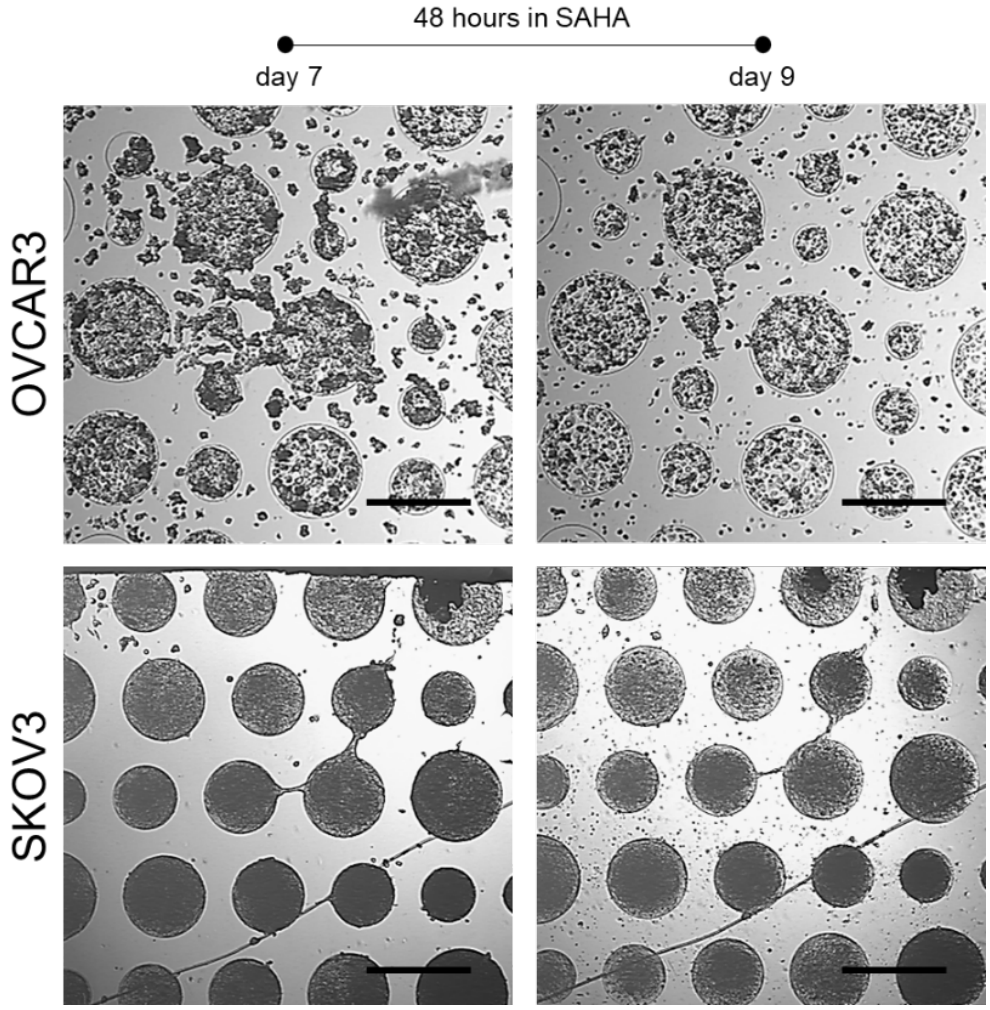

Figure 20. Representative images of OVCAR3 monolayers and SKOV3 aggregates before and after SAHA treatment. (scale bar = 500 μm).

In addition to immunofluorescent staining, RT qPCR was performed on OVCAR3 and SKOV3 cells before and after SAHA treatment on the substrates. Figure 21 shows that there is a significant upregulation in epithelial markers Claudin 8 and E-Cadherin in SKOV3 cells, as well as significant downregulation in mesenchymal markers MMP2, vimentin and N-Cadherin. No such observations are made in OVCAR3

suggesting that a change in phenotype occurs in SKOV3 after treatment with SAHA, resulting in a more epithelial like phenotype.

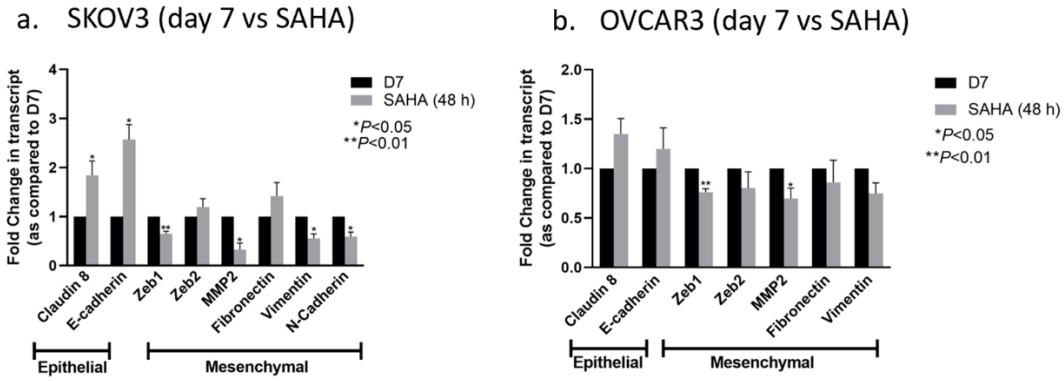

Figure 21. qPCR analysis of cells cultured on Si-TiB_2 substrates on day 7 before SAHA treatment and day 9 after 48 hours of SAHA treatment (mean expression with standard error bars, qPCR performed in triplicate for each experiment, from n>3 experiments per condition). (A) SKOV3 aggregates (B) OVCAR3 monolayers

These results are consistent with the immunofluorescent images of vimentin staining before and after SAHA treatment in SKOV3 which shows a qualitative (Figure 22) and quantitative (Figure 24) decrease in vimentin expression post SAHA treatment (p= 0.07495) while vimentin expression in aggregates returned to regular media after SAHA treatment showed a slight increase from day 7 do day 9 however this was not found to be significant (p=0.09095).

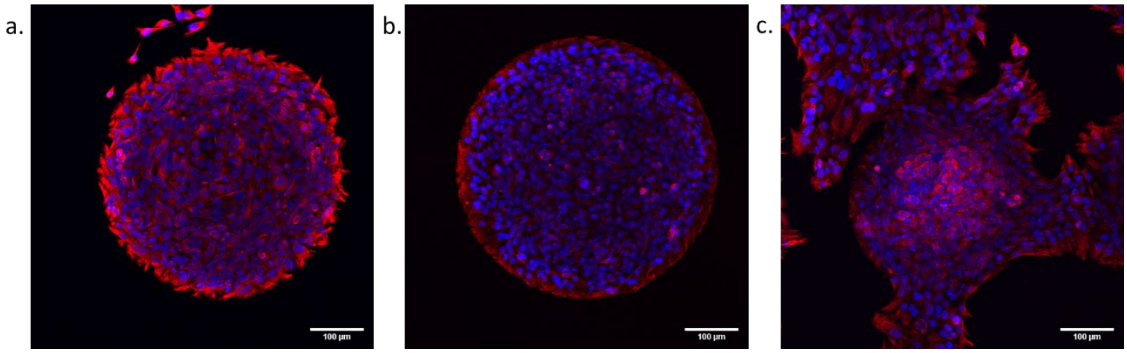

Figure 22. SKOV3 aggregates stained for vimentin and nuclei (DAPI) (scale bar = 100 µm). (A) day 7 (B) day 9 after 48 hour SAHA treatment (C) day 11 after returning SAHA treated aggregate to undrugged media

Since SAHA does not impact cell viability of the remaining cells we assessed its' impact on cell specificity after treatment by returning OVCAR3 and SKOV3 cells on Si-TiB_2 substrates to undrugged media for 48 hours, shown in Figure 23 [13]. Both cell lines had begun growing on the Si background by day 11.

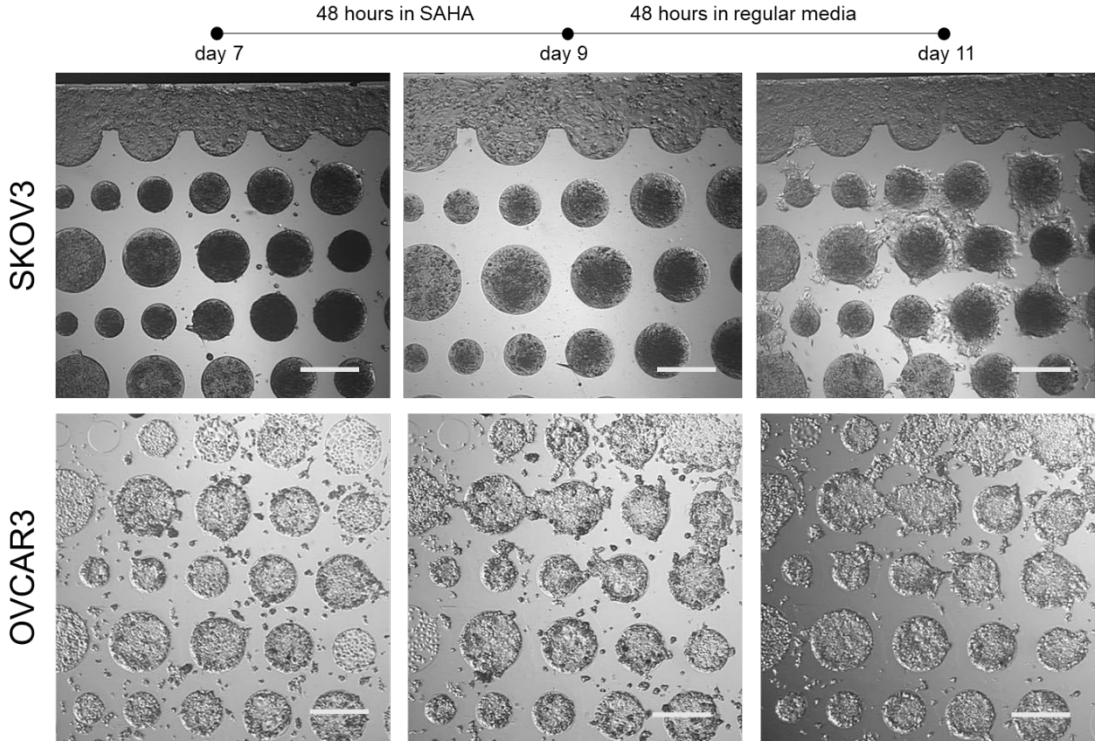

Figure 23. Representative stereomicroscopy images of cells on Si-TiB_2 substrates, drugged with SAHA on day 7 for 48 hours and returned to regular media on day 9 for 48 hours (scale bar = 500 μm).

We have previously observed by day 7 OVCAR3 cells have begun to lose preference for the TiB_2 background and by day 14 they have formed a solid monolayer across the patterned substrate. However, SKOV3 has been observed to remain relatively specific to TiB_2 patterns through day 14 under normal culturing conditions, as seen in Figure 12. Additionally, vimentin expression under these drug treatment conditions was analyzed. SKOV3 aggregates that were treated with SAHA and returned to regular media showed a downregulation in vimentin expression that was maintained 48 hours

after SAHA treatment ended as seen in Figure 24 and in representative image in Figure 22. Although the statistical analysis of vimentin expression from Immunofluorescent images was not found to be significant ($p=0.253$), the qPCR data shown in Figure 21 confirms that this trend is significant ($p<0.05$). These results suggest a connection between SAHA treatment and phenotype.

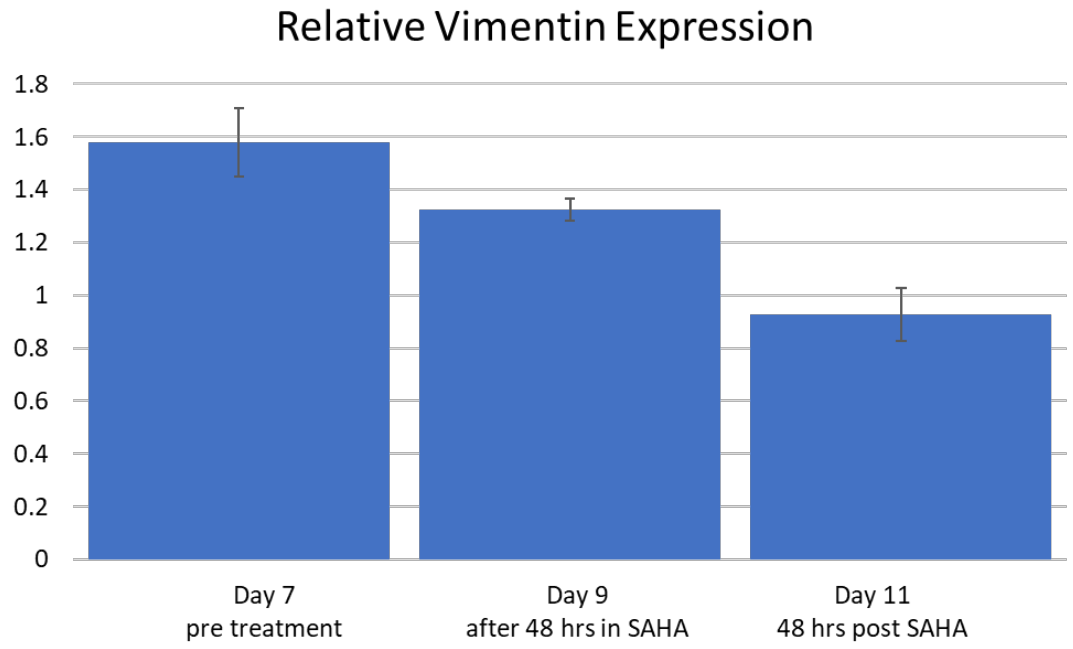

Figure 24. Mean relative vimentin expression (unitless) in SKOV3 aggregates before, during and after SAHA treatment with standard error bars. Normalized using DAPI (n>3 replicates, with >3 aggregates sampled per experiment). (day 7 vs. SAHA p=0.07495, day 7 vs. SAHA + regular media p=0.3642, SAHA vs. SAHA + regular media p=0.09095)

Staining of F-actin in the SKOV3 cells that overgrew onto the Si background on day 11 shows that they do retain their spindle like morphology and do not take on an epithelial rounded morphology (Figure 25).

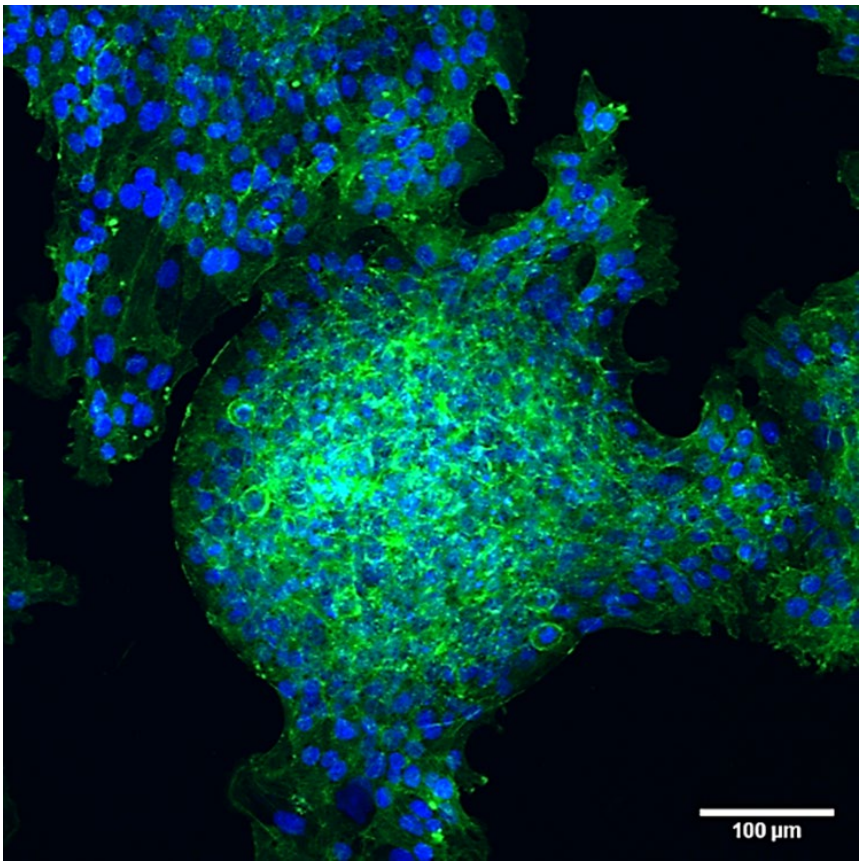

Figure 25. SKOV3 aggregate stained for F-actin and nuclei (DAPI) on day 11 after SAHA treatment and 48 hours in undrugged media (scale bar = 100 µm).

3.3.2 Combinatorial treatment

As previously mentioned, SAHA is known to enhance the effectiveness of some chemotherapeutics, and there have been a few studies into the possibility of combining SAHA and Paclitaxel as a potential therapeutic treatment for EOC. We hoped to assess the effects of this combination on EOC on our Si-TiB_2 platform. We therefore treated SKOV3 cells first with SAHA on day 7 of culture as previously described for 48 hours, and then followed this treatment with 48 hours of 0.05 µM Paclitaxel treatment. Initial results did not yield obvious visible differences in treatment conditions; therefore, the cells were allowed to continue growing in in undrugged media for 96 hours to further assess the long term effects of this treatment. Figure 26 shows the effects of the SAHA

+ Paclitaxel treatment as well as the control treatment of Paclitaxel alone on day 9 on SKOV3 aggregates. After allowing treated cells to grow in undrugged media for 96 hours visible differences are present between treatment conditions. Aggregates treated with the combination of drugs are visibly smaller than those only treated with Paclitaxel. The aggregate dimensions at day 7 before treatment and day 15 under the two treatment conditions were obtained using the macro for confocal IF images to determine aggregate thickness and diameter. A decrease in aggregate thickness was observed after SAHA + Paclitaxel ($p=4.006e-05$) and Paclitaxel only ($p=3.183E-07$) treatment, however the differences between treatment conditions were not statistically significant ($p=0.6084$). The same trend was observed in diameter measurements, showing a statistically significant decrease in aggregate diameter after treatment with SAHA + Paclitaxel ($p=0.005774$) and Paclitaxel only ($p=0.02302$) while comparisons at day 15 of the two treatment conditions did not show a statistically significant difference in aggregate diameter ($p=0.3440$).

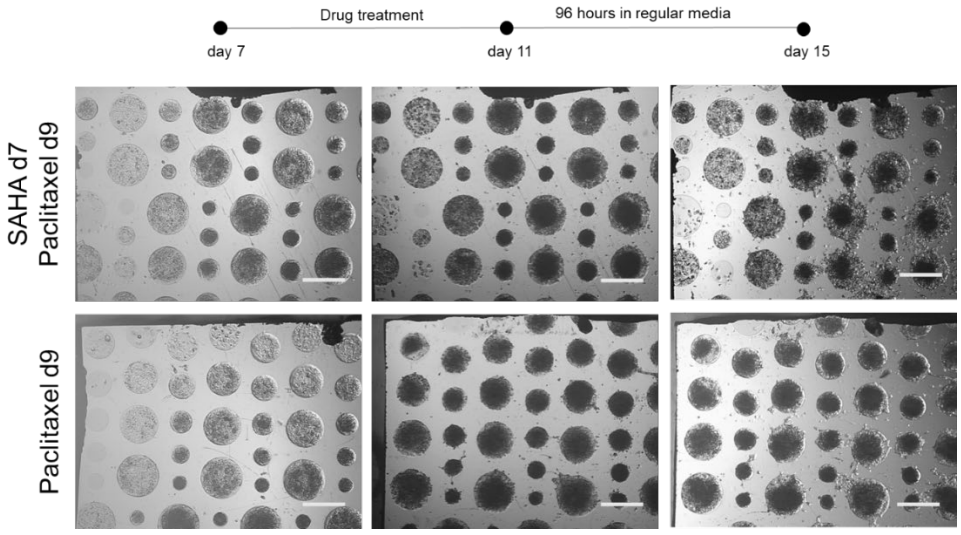

Figure 26. Representative stereomicroscopy images of SKOV3 aggregates treated with either SAHA on day 7 and Paclitaxel on day 9 or Paclitaxel alone on day 9. After drug treatment substrates were returned to undrugged media for 96 hours (scale bar = 500 μm).

In order to assess the effects of the combination treatment, cellular proliferation was measured using the Ki67 marker, shown in Figure 27. Unlike the SKOV3 treated only with SAHA, where overgrowth is seen when returned to culture media, SKOV3 aggregates treated with SAHA on day 7 followed by Paclitaxel on day 9 continue to shrink after drug treatment, while those treated with Paclitaxel alone maintain their aggregated shape as seen in Figure 26. Analysis of SKOV3 aggregates treated with the combination treatment after which they were allowed to culture for 96 hours maintain a lowered Ki67 expression, therefore a lower cellular proliferation over time after treatment.

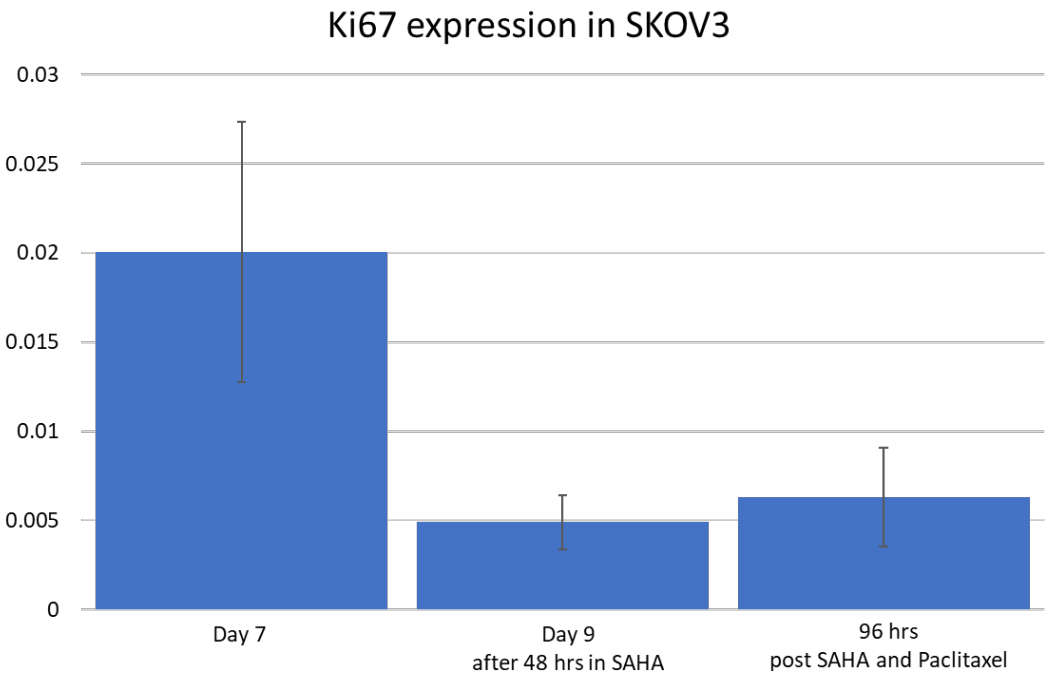

Figure 27. Mean relative expression of Ki67 in SKOV3 cells under varying conditions, normalized using DAPI pixel count with standard error bars (n>3 replicates, with >3 aggregates sampled per experiment). (day 7 vs. SAHA p=0.03515, day 7 vs. SAHA + Paclitaxel p=0.05490, SAHA vs. SAHA + Paclitaxel p=0.3321)

Although the shrinkage of SKOV3 aggregates treated with SAHA + Paclitaxel appeared to be more rapid than those treated with Paclitaxel only, statistical analysis of

the diameters of these aggregates, shown in Figure 28, revealed no significant difference between treatment groups (p=0.3440).

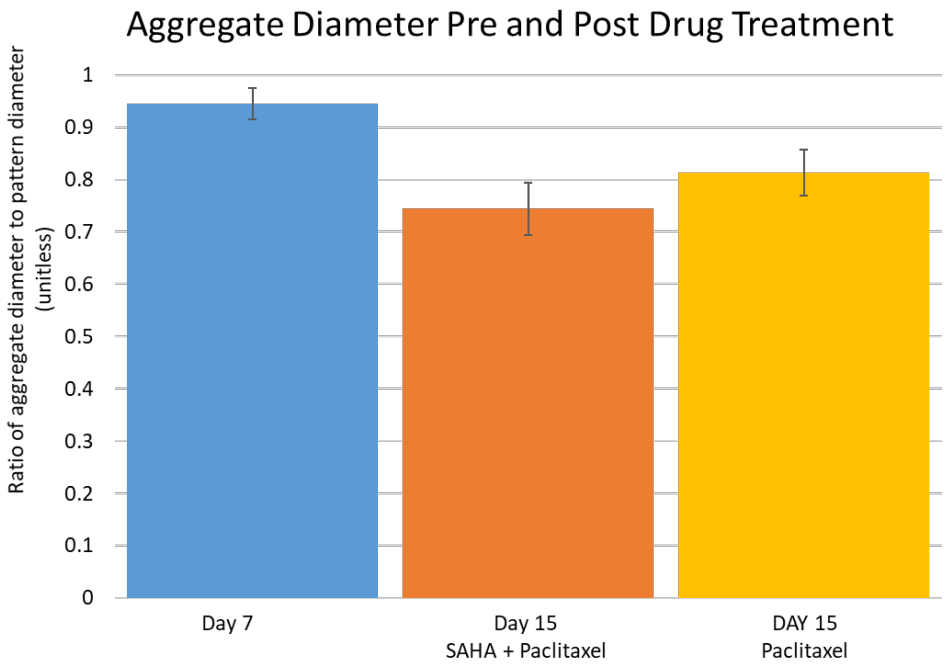

Figure 28. Mean diameter of SKOV3 aggregates pre and post drug treatment with standard error bars (n>3 replicates, with >3 aggregates sampled per experiment). (A) day 7 before treatment. (B) Day 15, 96 hours after the end of SAHA + Paclitaxel treatment. (C) Day 15, 96 hours after the end of Paclitaxel treatment.

Further qPCR analysis of SKOV3 cells treated with Paclitaxel only vs SAHA + Paclitaxel reveal a lower level of vimentin expression in SKOV3 cells that received the combination treatment, however these results were not significant (p=0.08345) as seen in Figure 29. Additionally, E-cadherin expression was not statistically different between treatment groups (Figure 29).

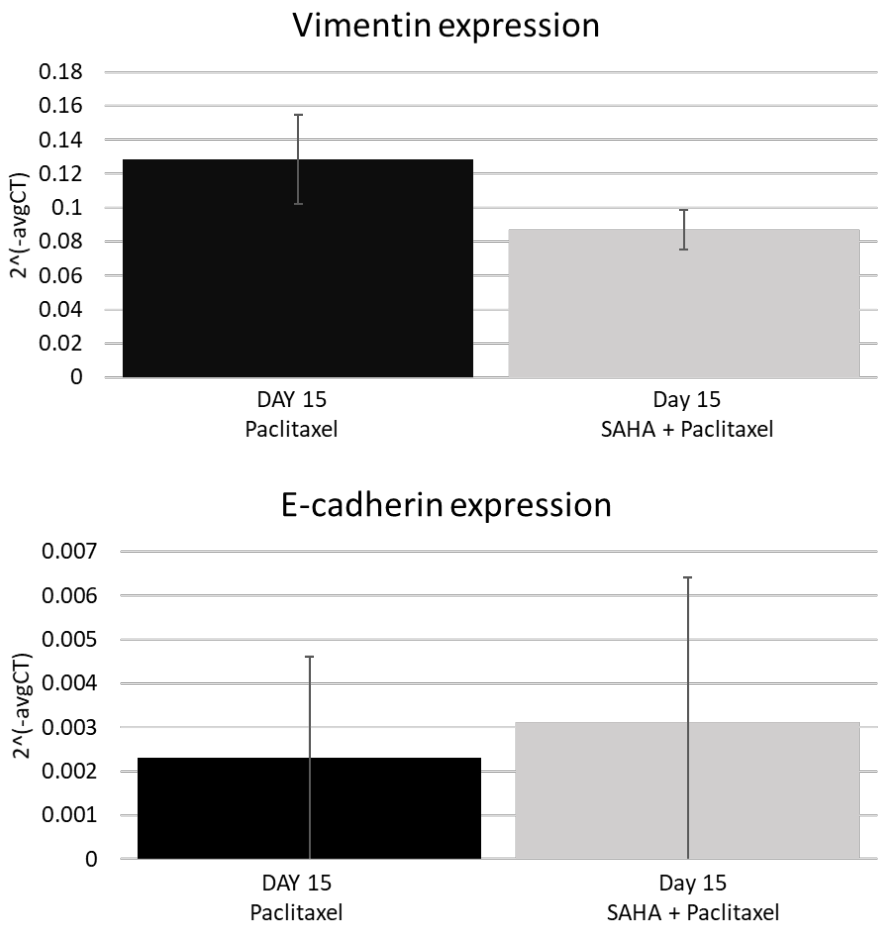

Figure 29. Mean expression of phenotypic markers in SKOV3 aggregates treated with SAHA + Paclitaxel vs Paclitaxel only via qPCR assay of mesenchymal marker vimentin and epithelial marker E-cadherin expression with standard error bars (qPCR performed in triplicate for each experiment, from n>3 experiments per condition).

Chapter 4 Discussion and Conclusion

This study functions as a proof of concept for the use of the Si-TiB_2 substrate for the study of epithelial ovarian cancer (EOC) of the mesenchymal subtype as they can form compact aggregates. We have shown that this substrate can facilitate studies of EOC in the third dimension using only typical cell culturing components and techniques.

This platform captures the aggregation and subsequent disaggregation of SKOV3 spheroids in the presence of SAHA and Paclitaxel. Whereas OVCAR3 cells

failed to aggregate, as also observed in other studies wherein SKOV3 cells were shown to form tight aggregates while OVCAR3 grew in loose sheets [42], [43].

The culturing of SKOV3 and OVCAR3 cells on these substrates reveals an immediate difference in phenotype that is visible in simple stereomicroscopy images. The dimensions of SKOV3 aggregates were dependent on diameter of the micropattern with diameters ranging from 120-490 μm. The thickness of the aggregates was less variable and independent of pattern size ranging from roughly 40 to 90 μm. However, the viability of these aggregates was also constant at approximately 85%. These parameters are in line with lower dimensions seen in in-*vivo* conditions, where EOC spheroids from the ascites are typically in the range of 50-700 μm in diameter and are highly viable, similar to the aggregates formed on our platform [42]–[45]. These findings suggest that our platform is a biologically relevant model that is competitive with commercially available models [43], [51]–[54].

Suberoylanilide hydroxamic acid (SAHA) is a histone deacetylase inhibitor that is believed to promote apoptosis through the arrest of the cell cycle at the G2/S phase by preferentially promoting tumor suppressor genes [14]. Some studies show that SAHA is selective to cancer cells and has no cytotoxic effect on non-cancerous cells [9], [11], [15]. Although this is promising for targeted therapy, the effects of SAHA on EOC cells is not believed to be strong enough to kill them as individual therapy has shown limited results. However, studies suggest that SAHA would be a good option as an additional therapy to augment the effects of chemotherapeutics [9], [11], [13]–[15], [38].

In this study, we demonstrated the disaggregation effects of SAHA on SKOV3 and OVCAR3 aggregates cultured on Si-TiB_2 micropatterned substrates. Despite this effect, there was no decrease in the viability of SKOV3 aggregates and when returned to undrugged media the SKOV3 cells lost their specificity and spheroid organization, growing in monolayers on the Si substrate background. This change in specificity was not seen when aggregates were treated with Paclitaxel alone or in combination with SAHA, suggesting that this overgrowth was not simply a result of alterations in proteins and growth factors present on the surface of the substrate over time.

Differences in vimentin expression of cells before and after SAHA treatment were assessed using immunofluorescence staining. While SAHA had no effect on the viability of either cell line, it downregulated mesenchymal marker vimentin in SKOV3 cells. Also, upon returning SAHA treated cells to regular media, the previously mesenchymal SKOV3 then displayed epithelial phenotypic markers and growth patterns similar to those seen in untreated OVCAR3 cells, however individual cell morphology was not altered.

Additionally, phenotypic characterization was performed using qPCR. SKOV3 cells showed increased expression of claudin 8 and E-cadherin (epithelial markers) and downregulation of MMP2, vimentin and N-cadherin (mesenchymal markers) further supporting the understanding that SAHA induces an epithelial phenotype through downregulation of vimentin [13].

The combination of SAHA and Paclitaxel treatment in SKOV3 cells showed a decreased proliferation (Ki67) immediately after SAHA treatment that was maintained 96 hours after Paclitaxel treatment ended, meaning that this decrease in proliferation

was maintained over time. Qualitative results showed more rapid shrinkage in aggregates treated with SAHA + Paclitaxel than those aggregates treated only with Paclitaxel, however statistical analysis of aggregate dimensions and phenotypic analysis demonstrate little difference in aggregates treated with Paclitaxel alone vs. SAHA + Paclitaxel. These finding suggest that SAHA may not augment the cytotoxic effects of Paclitaxel, however it is possible that the length of observation after treatment needs to be longer to observe significant differences between treatment groups.

In EOC, one of the main barriers to effective treatment is the resistance of many patients' cancers to chemotherapeutics like Paclitaxel [8]. Since this platform facilitates the study of 3D aggregates it more accurately mimics the conditions *in-vivo* which enables the study of chemotherapeutic resistance more accurately as cells in 2D culture are not as resistant to drug treatment which is not accurate to conditions in the body [23]–[26]. Additionally, the 2D structure of the Si-TiB_2 platform itself facilitates monitoring of phenotypic changes as morphology and growth patterns can change in response to treatments, as seen in SKOV3 aggregates treated with SAHA.

Importantly, attempts to culture OVCAR3 on this platform do not show promising results for studying 3D aggregated cells as this epithelial line does not exhibit strong aggregation. These results are consistent with other studies that show OVCAR3 is a non-aggregating EOC line [42]. We did not observe significant changes in phenotype of the OVCAR3 cells in the presence of SAHA as we did with SKOV3, which again suggests that SAHA effectively causes cells to move towards, or in the case of OVCAR3, case maintain an epithelial phenotype.

Overall, this study validates the use of the novel Si-TiB_2 substrate for the study of the mesenchymal SKOV3 EOC cell line, and potentially other mesenchymal cell lines in the future. This study highlights the platform's ability to culture primary tumor spheroid-like models of mesenchymal cell lines, monitor cell growth and capture changes in phenotype. Further studies into alterations of the platform for the culture of cells of varying phenotypes in order to study cancers of all phenotypes would be beneficial to the field of EOC research. Designing a 2D platform whose surface is easily altered to facilitate different studies has the potential to revolutionize the study of cancer and its therapeutic treatments.

Chapter 5 Future Work

Future work using this Si-TiB_2 micropatterned substrate platform could include longer assessments of Paclitaxel treatments in SKOV3 cells with or without SAHA in order to determine whether there are long-term differences between treatment groups. Furthermore, performing these experiments with patient derived cells or immortalized cell line with demonstrated resistance to Paclitaxel would allow for further understanding is SAHA's role in chemotherapeutic treatment.

Additionally, inducing EMT in SKOV3 cells using media supplemented with EMT factors on these micropatterned substrates would allow for further characterization of the EMT process in SKOV3 cells. This would allow for comparisons between the changes seen in SKOV3 treated with SAHA to further confirm that the drug does induce an epithelial phenotype.

REFERENCES

[1] F. Bray, J. Ferlay, I. Soerjomataram, R. L. Siegel, L. A. Torre, and A. Jemal, "Global cancer statistics 2018: GLOBOCAN estimates of incidence and mortality worldwide for 36 cancers in 185 countries," *CA. Cancer J. Clin.*, vol. 68, no. 6, pp. 394–424, 2018, doi: 10.3322/caac.21492.

[2] V. L. Beesley, T. L. Ross, M. T. King, R. Campbell, C. M. Nagle, A. Obermair, P. Grant, A. DeFazio, P. M. Webb, and M. L. Friedlander, "Evaluating patient-reported symptoms and late adverse effects following completion of first-line chemotherapy for ovarian cancer using the MOST (Measure of Ovarian Symptoms and Treatment concerns)," *Gynecol. Oncol.*, vol. 164, no. 2, pp. 437–445, Feb. 2022, doi: 10.1016/j.ygyno.2021.12.006.

[3] O. Bilyk, M. Coatham, M. Jewer, and L.-M. Postovit, "Epithelial-to-Mesenchymal Transition in the Female Reproductive Tract: From Normal Functioning to Disease Pathology," *Front. Oncol.*, vol. 7, p. 145, Jul. 2017, doi: 10.3389/fonc.2017.00145.

[4] S. M. Temkin, M. P. Smeltzer, M. D. Dawkins, L. M. Boehmer, L. Senter, D. R. Black, S. V. Blank, A. Yemelyanova, A. M. Magliocco, M. A. Finkel, T. E. Moore, and P. H. Thaker, "Improving the quality of care for patients with advanced epithelial ovarian cancer: Program components, implementation barriers, and recommendations," *Cancer*, vol. 128, no. 4, pp. 654–664, Feb. 2022, doi: 10.1002/cncr.34023.

[5] “Ovary - Epithelial Carcinoma.” http://www.bccancer.bc.ca/health-professionals/clinical-resources/cancer-management-manual/gynecology/ovary-epithelial-carcinoma (accessed Apr. 13, 2022).

[6] “Ovarian Cancer Stages, Survival Rate and Prognosis,” *OCRA*. https://ocrahope.org/patients/about-ovarian-cancer/staging/ (accessed Apr. 13, 2022).

[7] “Ovarian Cancer | Patient Care.” https://weillcornell.org/services/obstetrics-and-gynecology/gynecologic-oncology/conditions-we-treat/ovarian-cancer (accessed Apr. 13, 2022).

[8] M. Alharbi, S. Sharma, D. Guanzon, A. Lai, F. Zuñiga, M. J. A. Shiddiky, Y. Yamauchi, A. Salas-Burgos, Y. He, T. Pejovic, C. Winters, T. Morgan, L. Perrin, J. D. Hooper, and C. Salomon, “miRNa signature in small extracellular vesicles and their association with platinum resistance and cancer recurrence in ovarian cancer,” *Nanomedicine Nanotechnol. Biol. Med.*, vol. 28, p. 102207, Aug. 2020, doi: 10.1016/j.nano.2020.102207.

[9] J. Sonnemann, J. Gänge, S. Pilz, C. Stötzer, R. Ohlinger, A. Belau, G. Lorenz, and J. F. Beck, “Comparative evaluation of the treatment efficacy of suberoylanilide hydroxamic acid (SAHA) and paclitaxel in ovarian cancer cell lines and primary ovarian cancer cells from patients,” *BMC Cancer*, vol. 6, p. 183, Jul. 2006, doi: 10.1186/1471-2407-6-183.

[10] R. Januchowski, K. Wojtowicz, P. Sujka-Kordowska, M. Andrzejewska, and M. Zabel, “MDR gene expression analysis of six drug-resistant ovarian cancer cell lines,” *BioMed Res. Int.*, vol. 2013, p. 241763, 2013, doi: 10.1155/2013/241763.

[11] J. Li, D. Hao, L. Wang, H. Wang, Y. Wang, Z. Zhao, P. Li, C. Deng, and L. Di, “Epigenetic targeting drugs potentiate chemotherapeutic effects in solid tumor therapy,” *Sci. Rep.*, vol. 7, no. 1, Art. no. 1, Jun. 2017, doi: 10.1038/s41598-017-04406-0.

[12] P. A. Konstantinopoulos, A. J. Wilson, J. Saskowski, E. Wass, and D. Khabele, “Suberoylanilide Hydroxamic Acid (SAHA) enhances olaparib activity by targeting homologous recombination DNA repair in ovarian cancer,” *Gynecol. Oncol.*, vol. 133, no. 3, pp. 599–606, Jun. 2014, doi: 10.1016/j.ygyno.2014.03.007.

[13] A. Wawruszak, L. Borkiewicz, E. Okon, W. Kukula-Koch, S. Afshan, and M. Halasa, “Vorinostat (SAHA) and Breast Cancer: An Overview,” *Cancers*, vol. 13, no. 18, p. 4700, Sep. 2021, doi: 10.3390/cancers13184700.

[14] M.-Y. Chen, W. S.-L. Liao, Z. Lu, W. G. Bornmann, V. Hennessey, M. N. Washington, G. L. Rosner, Y. Yu, A. A. Ahmed, and R. C. Bast Jr., “Decitabine and suberoylanilide hydroxamic acid (SAHA) inhibit growth of ovarian cancer cell lines and xenografts while inducing expression of imprinted tumor suppressor genes, apoptosis, G2/M arrest, and autophagy,” *Cancer*, vol. 117, no. 19, pp. 4424–4438, 2011, doi: 10.1002/cncr.26073.

[15] Z. Liu, Y. Tong, Y. Liu, H. Liu, C. Li, Y. Zhao, and Y. Zhang, “Effects of suberoylanilide hydroxamic acid (SAHA) combined with paclitaxel (PTX) on paclitaxel-resistant ovarian cancer cells and insights into the underlying mechanisms,” *Cancer Cell Int.*, vol. 14, no. 1, p. 112, Nov. 2014, doi: 10.1186/s12935-014-0112-x.

[16] C. S. Dietrich, V. L. Greenberg, C. P. DeSimone, S. C. Modesitt, J. R. van Nagell, R. Craven, and S. G. Zimmer, "Suberoylanilide hydroxamic acid (SAHA) potentiates paclitaxel-induced apoptosis in ovarian cancer cell lines," *Gynecol. Oncol.*, vol. 116, no. 1, pp. 126–130, Jan. 2010, doi: 10.1016/j.ygyno.2009.09.039.

[17] A. L. Cooper, V. L. Greenberg, P. S. Lancaster, J. R. van Nagell, S. G. Zimmer, and S. C. Modesitt, "In vitro and in vivo histone deacetylase inhibitor therapy with suberoylanilide hydroxamic acid (SAHA) and paclitaxel in ovarian cancer," *Gynecol. Oncol.*, vol. 104, no. 3, pp. 596–601, Mar. 2007, doi: 10.1016/j.ygyno.2006.09.011.

[18] Merck Sharp & Dohme Corp., "A Clinical Trial of Vorinostat (MK0683, SAHA) in Combination With FDA Approved Cancer Drugs in Patients With Advanced Non-Small Cell Lung Cancer (NSCLC)(0683-056)," NCT00473889, Jul. 2015.

[19] M. A. Nieto, R. Y.-J. Huang, R. A. Jackson, and J. P. Thiery, "EMT: 2016," *Cell*, vol. 166, no. 1, pp. 21–45, Jun. 2016, doi: 10.1016/j.cell.2016.06.028.

[20] L. G. Hudson, R. Zeineldin, and M. S. Stack, "Phenotypic plasticity of neoplastic ovarian epithelium: unique cadherin profiles in tumor progression," *Clin. Exp. Metastasis*, vol. 25, no. 6, pp. 643–655, 2008, doi: 10.1007/s10585-008-9171-5.

[21] A. Kumari, Z. Shonibare, M. Monavarian, R. C. Arend, N. Y. Lee, G. J. Inman, and K. Mythreye, "TGFβ signaling networks in ovarian cancer progression and plasticity," *Clin. Exp. Metastasis*, vol. 38, no. 2, pp. 139–161, Apr. 2021, doi: 10.1007/s10585-021-10077-z.

[22] M. M. Nijkamp, P. N. Span, I. J. Hoogsteen, A. J. van der Kogel, J. H. A. M. Kaanders, and J. Bussink, "Expression of E-cadherin and vimentin correlates with metastasis formation in head and neck squamous cell carcinoma patients," *Radiother. Oncol. J. Eur. Soc. Ther. Radiol. Oncol.*, vol. 99, no. 3, pp. 344–348, Jun. 2011, doi: 10.1016/j.radonc.2011.05.066.

[23] C. Jensen and Y. Teng, "Is It Time to Start Transitioning From 2D to 3D Cell Culture?," *Front. Mol. Biosci.*, vol. 7, 2020, Accessed: Apr. 11, 2022. [Online]. Available: https://www.frontiersin.org/article/10.3389/fmolb.2020.00033

[24] E. J. Brock, K. Ji, S. Shah, R. R. Mattingly, and B. F. Sloane, "In Vitro Models for Studying Invasive Transitions of Ductal Carcinoma In Situ," *J. Mammary Gland Biol. Neoplasia*, vol. 24, no. 1, pp. 1–15, Mar. 2019, doi: 10.1007/s10911-018-9405-3.

[25] P. Friedl and S. Alexander, "Cancer invasion and the microenvironment: plasticity and reciprocity," *Cell*, vol. 147, no. 5, pp. 992–1009, Nov. 2011, doi: 10.1016/j.cell.2011.11.016.

[26] M. Lintz, A. Muñoz, and C. A. Reinhart-King, "The Mechanics of Single Cell and Collective Migration of Tumor Cells," *J. Biomech. Eng.*, vol. 139, no. 2, Feb. 2017, doi: 10.1115/1.4035121.

[27] X. Wu, J. Su, J. Wei, N. Jiang, and X. Ge, "Recent Advances in Three-Dimensional Stem Cell Culture Systems and Applications," *Stem Cells Int.*, vol. 2021, p. 9477332, Oct. 2021, doi: 10.1155/2021/9477332.

[28] J. Friguglietti, S. Das, P. Le, D. Fraga, M. Quintela, S. A. Gazze, D. McPhail, J. Gu, O. Sabek, A. O. Gaber, L. W. Francis, W. Zagozdzon-Wosik, and F. A.

Merchant, “Novel Silicon Titanium Diboride Micropatterned Substrates for Cellular Patterning,” *Biomaterials*, vol. 244, p. 119927, Jun. 2020, doi: 10.1016/j.biomaterials.2020.119927.

[29] H.-H. Huang, C.-T. Ho, T.-H. Lee, T.-L. Lee, K.-K. Liao, and F.-L. Chen, “Effect of surface roughness of ground titanium on initial cell adhesion,” *Biomol. Eng.*, vol. 21, no. 3, pp. 93–97, Nov. 2004, doi: 10.1016/j.bioeng.2004.05.001.

[30] A. Zareidoost, M. Yousefpour, B. Ghaseme, and A. Amanzadeh, “The relationship of surface roughness and cell response of chemical surface modification of titanium,” *J. Mater. Sci. Mater. Med.*, vol. 23, no. 6, pp. 1479–1488, Jun. 2012, doi: 10.1007/s10856-012-4611-9.

[31] T. Spivak-Kroizman, M. A. Lemmon, I. Dikic, J. E. Ladbury, D. Pinchasi, J. Huang, M. Jaye, G. Crumley, J. Schlessinger, and I. Lax, “Heparin-induced oligomerization of FGF molecules is responsible for FGF receptor dimerization, activation, and cell proliferation,” *Cell*, vol. 79, no. 6, pp. 1015–1024, Dec. 1994, doi: 10.1016/0092-8674(94)90032-9.

[32] M. Presta, G. Andrés, D. Leali, P. Dell’Era, and R. Ronca, “Inflammatory cells and chemokines sustain FGF2-induced angiogenesis,” *Eur. Cytokine Netw.*, vol. 20, no. 2, pp. 39–50, Jun. 2009, doi: 10.1684/ecn.2009.0155.

[33] A. Levine, G. Kenet, R. Bruck, Y. Avni, I. Avinoach, H. Aeed, Z. Matas, M. David, and A. Yayon, “Effect of Heparin on Tissue Binding Activity of Fibroblast Growth Factor and Heparin-Binding Epidermal Growth Factor in Experimental Colitis in Rats,” *Pediatr. Res.*, vol. 51, no. 5, Art. no. 5, May 2002, doi: 10.1203/00006450-200205000-00015.

[34] L. A. Chandler, B. A. Sosnowski, L. Greenlees, S. L. Aukerman, A. Baird, and G. F. Pierce, “Prevalent expression of fibroblast growth factor (FGF) receptors and FGF2 in human tumor cell lines,” *Int. J. Cancer*, vol. 81, no. 3, pp. 451–458, May 1999, doi: 10.1002/(sici)1097-0215(19990505)81:3<451::aid-ijc20>3.0.co;2-h.

[35] D. McPhail, “Titanium diboride bioMEMS; investigating ovarian cancer spheroid formation in the presence of epigenomic instability.,” 2019.

[36] N. Gavara, “A beginner’s guide to atomic force microscopy probing for cell mechanics,” *Microsc. Res. Tech.*, vol. 80, no. 1, pp. 75–84, Jan. 2017, doi: 10.1002/jemt.22776.

[37] F. Alshamsi, “Investigation of Ovarian Cancer Spheroid Formation and Disaggregation in the Presence of Epigenomic Instability on Novel Micropatterned Substrate.,” 2020.

[38] S. Chen, Y. Zhao, W. Gou, S. Zhao, Y. Takano, and H. Zheng, “The Anti-Tumor Effects and Molecular Mechanisms of Suberoylanilide Hydroxamic Acid (SAHA) on the Aggressive Phenotypes of Ovarian Carcinoma Cells,” *PLOS ONE*, vol. 8, no. 11, p. e79781, Nov. 2013, doi: 10.1371/journal.pone.0079781.

[39] H. Huang, Y. Fu, Y. Zhang, F. Peng, M. Lu, Y. Feng, L. Chen, Z. Chen, M. Li, and Y. Chen, “Dissection of Anti-tumor Activity of Histone Deacetylase Inhibitor SAHA in Nasopharyngeal Carcinoma Cells via Quantitative Phosphoproteomics,” *Front. Cell Dev. Biol.*, vol. 8, 2020, Accessed: Apr. 13, 2022. [Online]. Available: https://www.frontiersin.org/article/10.3389/fcell.2020.577784

[40] N. Takai and H. Narahara, “Histone deacetylase inhibitor therapy in epithelial ovarian cancer,” *J. Oncol.*, vol. 2010, p. 458431, 2010, doi: 10.1155/2010/458431.

[41] N. Takai, N. Kawamata, D. Gui, J. W. Said, I. Miyakawa, and H. P. Koeffler, “Human ovarian carcinoma cells: histone deacetylase inhibitors exhibit antiproliferative activity and potently induce apoptosis,” *Cancer*, vol. 101, no. 12, pp. 2760–2770, Dec. 2004, doi: 10.1002/cncr.20709.

[42] K. L. Sodek, M. J. Ringuette, and T. J. Brown, “Compact spheroid formation by ovarian cancer cells is associated with contractile behavior and an invasive phenotype,” *Int. J. Cancer*, vol. 124, no. 9, pp. 2060–2070, 2009, doi: 10.1002/ijc.24188.

[43] S. Raghavan, M. R. Ward, K. R. Rowley, R. M. Wold, S. Takayama, R. J. Buckanovich, and G. Mehta, “Formation of stable small cell number three-dimensional ovarian cancer spheroids using hanging drop arrays for preclinical drug sensitivity assays,” *Gynecol. Oncol.*, vol. 138, no. 1, pp. 181–189, Jul. 2015, doi: 10.1016/j.ygyno.2015.04.014.

[44] A. J. McKenzie, S. R. Hicks, K. V. Svec, H. Naughton, Z. L. Edmunds, and A. K. Howe, “The mechanical microenvironment regulates ovarian cancer cell morphology, migration, and spheroid disaggregation,” *Sci. Rep.*, vol. 8, no. 1, Art. no. 1, May 2018, doi: 10.1038/s41598-018-25589-0.

[45] G. Gunay, H. A. Kirit, A. Kamatar, O. Baghdasaryan, S. Hamsici, and H. Acar, “The effects of size and shape of the ovarian cancer spheroids on the drug resistance and migration,” *Gynecol. Oncol.*, vol. 159, no. 2, pp. 563–572, Nov. 2020, doi: 10.1016/j.ygyno.2020.09.002.

[46] V. Heredia-Soto, A. Redondo, A. Berjón, M. Miguel-Martín, E. Díaz, R. Crespo, A. Hernández, L. Yébenes, A. Gallego, J. Feliu, D. Hardisson, and M. Mendiola, "High-throughput 3-dimensional culture of epithelial ovarian cancer cells as preclinical model of disease," *Oncotarget*, vol. 9, no. 31, pp. 21893–21903, Apr. 2018, doi: 10.18632/oncotarget.25098.

[47] M. Rosso, B. Majem, L. Devis, L. Lapyckyj, M. J. Besso, M. Llauradó, M. F. Abascal, M. L. Matos, L. Lanau, J. Castellví, J. L. Sánchez, A. P. Benavente, A. Gil-Moreno, J. Reventós, A. S. Margalef, M. Rigau, and M. H. Vazquez-Levin, "E-cadherin: A determinant molecule associated with ovarian cancer progression, dissemination and aggressiveness," *PLOS ONE*, vol. 12, no. 9, p. e0184439, Sep. 2017, doi: 10.1371/journal.pone.0184439.

[48] N. M. Aiello, R. Maddipati, R. J. Norgard, D. Balli, J. Li, S. Yuan, T. Yamazoe, T. Black, A. Sahmoud, E. E. Furth, D. Bar-Sagi, and B. Z. Stanger, "EMT Subtype Influences Epithelial Plasticity and Mode of Cell Migration," *Dev. Cell*, vol. 45, no. 6, pp. 681-695.e4, Jun. 2018, doi: 10.1016/j.devcel.2018.05.027.

[49] N. Loret, H. Denys, P. Tummers, and G. Berx, "The Role of Epithelial-to-Mesenchymal Plasticity in Ovarian Cancer Progression and Therapy Resistance," *Cancers*, vol. 11, no. 6, p. E838, Jun. 2019, doi: 10.3390/cancers11060838.

[50] X. Wu, J. Zhao, Y. Ruan, L. Sun, C. Xu, and H. Jiang, "Sialyltransferase ST3GAL1 promotes cell migration, invasion, and TGF-β1-induced EMT and confers paclitaxel resistance in ovarian cancer," *Cell Death Dis.*, vol. 9, no. 11, pp. 1–14, Oct. 2018, doi: 10.1038/s41419-018-1101-0.

[51] K. Duval, H. Grover, L.-H. Han, Y. Mou, A. F. Pegoraro, J. Fredberg, and Z. Chen, “Modeling Physiological Events in 2D vs. 3D Cell Culture,” *Physiol. Bethesda Md*, vol. 32, no. 4, pp. 266–277, Jul. 2017, doi: 10.1152/physiol.00036.2016.

[52] C. Zhang, Z. Yang, D.-L. Dong, T.-S. Jang, J. C. Knowles, H.-W. Kim, G.-Z. Jin, and Y. Xuan, “3D culture technologies of cancer stem cells: promising ex vivo tumor models,” *J. Tissue Eng.*, vol. 11, p. 2041731420933407, Dec. 2020, doi: 10.1177/2041731420933407.

[53] M. Kapałczyńska, T. Kolenda, W. Przybyła, M. Zajączkowska, A. Teresiak, V. Filas, M. Ibbs, R. Bliźniak, Ł. Łuczewski, and K. Lamperska, “2D and 3D cell cultures - a comparison of different types of cancer cell cultures,” *Arch. Med. Sci. AMS*, vol. 14, no. 4, pp. 910–919, Jun. 2018, doi: 10.5114/aoms.2016.63743.

[54] C. J. de Witte, J. Espejo Valle-Inclan, N. Hami, K. Lõhmussaar, O. Kopper, C. P. H. Vreuls, G. N. Jonges, P. van Diest, L. Nguyen, H. Clevers, W. P. Kloosterman, E. Cuppen, H. J. G. Snippert, R. P. Zweemer, P. O. Witteveen, and E. Stelloo, “Patient-Derived Ovarian Cancer Organoids Mimic Clinical Response and Exhibit Heterogeneous Inter- and Intrapatient Drug Responses,” *Cell Rep.*, vol. 31, no. 11, p. 107762, Jun. 2020, doi: 10.1016/j.celrep.2020.107762.